Miner Petrol (2015) 109:181–200
DOI 10.1007/s00710-014-0359-x

ORIGINAL PAPER

LA-ICP-MS mineral chemistry of titanite and the geological implications for exploration of porphyry Cu deposits in the Jinshajiang – Red River alkaline igneous belt, SW China

Leiluo Xu · Xianwu Bi · Ruizhong Hu · Yongyong Tang · Xinsong Wang · Yue Xu

Received: 8 July 2013 / Accepted: 5 November 2014 / Published online: 10 December 2014

Abstract The Jinshajiang–Red River alkaline igneous belt in the eastern Indian–Asian collision zone, of southwestern China, hosts abundant, economically important Cu–Mo–Au mineralization of Cenozoic age. Major- and trace-element compositions of titanites from representative Cu-mineralized intrusions determined by LA-ICP-MS show higher values for Fe_2O_3/Al_2O_3, ΣREE+Y, LREE/HREE, Ce/Ce*, (Ce/Ce*)/(Eu/Eu*), U, Th, Ta, Nb and Ga, and lower values for Al_2O_3, CaO, Eu/Eu*, Zr/Hf, Nb/Ta and Sr than those for titanites from barren intrusions. Different ΣREE+Y, LREE/HREE, U, Th, Ta and Nb values of titanites between Cu-mineralized and barren intrusions were controlled mainly by the coexisting melt compositions. However, different Sr concentrations and negative Eu anomalies of titanites between Cu-mineralized and barren intrusions were most probably caused by different degrees of crystallization of feldspar from melts. In addition, different Ga concentrations and positive Ce anomalies of titanites between Cu-mineralized and barren intrusions were most likely caused by different magmatic fO_2 conditions. Pronounced compositional differences of titanites between Cu-mineralized and barren intrusions can provide a useful tool to help discriminate between ore-bearing and barren intrusions at an early stage of exploration, and, thus, have a potential application in exploration for porphyry Cu deposits in the Jinshajiang – Red River alkaline igneous belt, and to other areas.

Editorial handling: L. Danyushevsky

Electronic supplementary material The online version of this article (doi:10.1007/s00710-014-0359-x) contains supplementary material, which is available to authorized users.

L. L. Xu · X. W. Bi (✉) · R. Z. Hu · Y. Y. Tang · X. S. Wang · Y. Xu
State Key Laboratory of Ore Deposit Geochemistry, Institute of Geochemistry, Chinese Academy of Sciences, Guiyang 550002, China
e-mail: bixianwu@vip.gyig.ac.cn

Y. Y. Tang · X. S. Wang · Y. Xu
Graduate University of Chinese Academy of Sciences, Beijing 100049, China

Introduction

Titanite ($CaTiSiO_5$) is a common accessory mineral in igneous and metamorphic rocks, and hydrothermal ore deposits (Frost et al. 2000; Li et al. 2010). Through chemical substitutions, titanite can concentrate significant amounts of REEs, U, Th, Sr, Y, Mn and Pb in the sevenfold Ca site (Higgins and Ribbe 1976; Deer et al. 1982; Tiepolo et al. 2002), and can also accommodate significant amounts of HFSEs, such as Nb, Ta, Zr and W, in the octahedral Ti site (Groat et al. 1985; Bernau and Franz 1987; Lucassen et al. 2011). To a large extent, variations in trace-element compositions of titanite reflect changes of relevant geological conditions, and thus titanite can act as an important indicator of geological processes (Frost et al. 2000; Smith et al. 2009; Ismail et al. 2013). In general, the stability filed of titanite expands in systems with high Ca/Al ratios and relatively oxidizing conditions (~FMQ+1<fO_2<~FMQ+2) (Frost et al. 2000), and the valence state of Ce in titanite records relatively high-fO_2 conditions (King et al. 2013). Titanite with high Fe/Al and Th/U ratios is generally darker in colour (Aleinikoff et al. 2002). Titanite, like zircon, can account for a large proportion of total REE present in the rock (Tiepolo et al. 2002; Vuorinen and Hålenius 2005; Buick et al. 2007; Marks et al. 2008), but titanite of magmatic origin commonly has a higher Th/U ratio than that for metamorphic titanite, which is different from zircon (Gao et al. 2012). Because titanite may incorporate appreciable amounts of U and Th into its structure and has a high closure temperature for Pb diffusion, it can be used as a U-Th-Pb geochronometer (Frost et al. 2000; Buick et al. 2007; Massimo et al. 2013). Zirconium in titanite is sensitive to

variations of temperature and pressure and thus can be used as an important thermobarometer (Hayden et al. 2008). Increasing number of studies have indicated that titanite can act as an important host for Sn, W and Mo, and thus prove useful in certifying Sn-, W- and Mo-enriched intrusions, and has a potential application for exploration of Sn, W and Mo deposits (Aleksandrov and Troneva 2007; Xie et al. 2010; Wang et al. 2012; Che et al. 2013).

The Jinshajiang–Red River alkaline igneous belt, extending for over 2000 km adjacent to the NNW–NW-trending Jinshajiang–Red River fault zone, is an important region of Cenozoic Cu–Mo–Au mineralization within the eastern Indo-Asian collision zone (Xu et al. 2012a). This belt contains several hundred alkaline intrusions (Zhang and Xie 1997; Chung et al. 1997, 1998), and dozens of magmatic-hydrothermal Cu–Mo–Au deposits including the Yulong Cu (Mo-Au) and Beiya Au-Pb-Zn deposits, which are associated with alkaline magmatism. While the relationship between individual ore deposits and localized, minor intrusions have been demonstrated (e.g., the Yulong and Machangqing Cu (Mo-Au) deposits, Hou et al. 2006; Xu et al. 2012a), the majority of the alkaline intrusions have not been studied in detail and their mineralization potential is unknown. Hence, a relatively rapid, convenient and economical method for distinguishing between barren and mineralized intrusion would be useful. In recent years, *in-situ* micro-analytical techniques such as laser ablation inductively coupled plasma mass spectrometry (LA-ICP-MS), have been applied widely to major- and trace-element analysis of various rock-forming and accessory minerals (Liu et al. 2008). Geochemical analyses by LA-ICP-MS of accessory minerals, such as zircon, apatite, titanite and rutite, have shown that accessory minerals can be key indicators of mineralization (Ballard et al. 2002; Belousova et al. 2002; Scott 2005; Liang et al. 2006a, b; Xie et al. 2010; Cao et al. 2012; Li et al. 2012; Wang et al. 2012; Che et al. 2013).

Titanite is a common accessory phase in the Jinshajiang–Red River alkaline intrusions. In this paper, we have determined the major- and trace-element compositions of titanites from several representative Cu-mineralized and barren intrusions within the Jinshajiang – Red River alkaline igneous belt. Our study is focused on understanding the mineral chemical characteristics of titanites from mineralized and barren intrusions, and discussing their geological implications for exploration of porphyry Cu deposits in the Jinshajiang – Red River alkaline igneous belt, and elsewhere.

Geological background

The Jinshajiang–Red River alkaline igneous belt extends for over 2000 km and is distributed along the NNW–NW-trending Jinshajiang–Red River deep fault zone along the eastern edge of the Tibetan plateau (Fig. 1; Zhang and Xie 1997; Chung et al. 1997, 1998). The Indo–Asian collision, starting at ~65 Ma, created the Tibetan plateau and resulted in the eastward extrusional tectonics facilitated by strike-slip motion along major faults (e.g., the Jiali, Batang–Lijiang, Gaoligong faults, etc.; Fig. 1), including the Jinshajiang–Red River fault. Strike-slip motion along the Jinshajiang–Red River fault caused lithospheric-scale extension and emplacement of numerous alkaline igneous rocks, including volcanic and intrusive rocks, in the 2000 km long and 50–80 km wide Jinshajiang–Red River alkaline igneous belt (Chung et al. 1997, 1998; Bi et al. 1999, 2009; Yin and Harrison 2000; Ding et al. 2003, 2005; Mo et al. 2003; 2008; Hou et al. 2006, 2007). These alkaline igneous rocks have zircon U–Pb ages between ~43 Ma and ~35 Ma (Xu 2011; Xu et al. 2012a). The rocks range in composition from basaltic to trachytic and rhyolitic (Chung et al. 1998), and are characterized by high alkali contents ($K_2O+Na_2O>8$ wt.%) and potassium enrichment ($K_2O/Na_2O>1$), allowing for their characterization as high-K calc-alkaline or shoshonitic series. Discoveries of abundant alkaline intrusion-associated porphyry Cu(Mo-Au) deposits in the Jinshajiang–Red River alkaline igneous belt make it one of the most important porphyry Cu (Mo-Au) ore belts of Cenozoic age in SW China (Bi et al. 1999, 2002, 2004, 2009; Hu et al. 1998, 2004; Gu et al. 2003; Wang et al. 2004; Hou et al. 2007, 2011; Xu et al. 2012a). Representative porphyry Cu (Mo-Au) deposits including the Yulong, Machangqing, Tongchang and Chang'anchong deposits, are distributed in the northern, central and southern segments of the belt, respectively (Fig. 1). In addition, there are many barren alkaline intrusions in the belt, and representative barren intrusions include the Liuhe, Songgui and Yanshuiqing intrusions in the central part of the belt (Fig. 1).

Yulong, Machangqing, Tongchang and Chang'anchong porphyry Cu (Mo-Au) deposits

The Yulong deposit is located in the north of the Jinshajiang–Red River alkaline igneous belt (Fig. 1). It is part of the Yulong porphyry copper belt which extends for over 400 km and contains porphyry Cu (Mo-Au) ore deposits with ages of 41–35 Ma, such as Narigongma, Yulong, Malasongduo, Duoxiasongduo, Zhanaga and Mangzong , and more than 20 other Cu (Au)-mineralized porphyries (Hou et al. 2003; Liang et al. 2006a; Xu et al. 2012a). The Yulong deposit is the largest in the Yulong belt, having reserves of ~6.5 Mt Cu and 0.15 Mt Mo with average grades of 0.38 wt.% Cu, 0.04 wt.% Mo, and 0.35 g/t Au (Xu et al. 2012a). Cu (Mo-Au)-mineralization at the Yulong deposit occurred within and around the ~41 Ma monzogranite porphyry stock with an outcrop area of 0.64 km^2 (Fig. 2a; Xu et al. 2012a), which intruded into Triassic sandstone and limestone (Li et al. 2012). The Yulong monzogranite

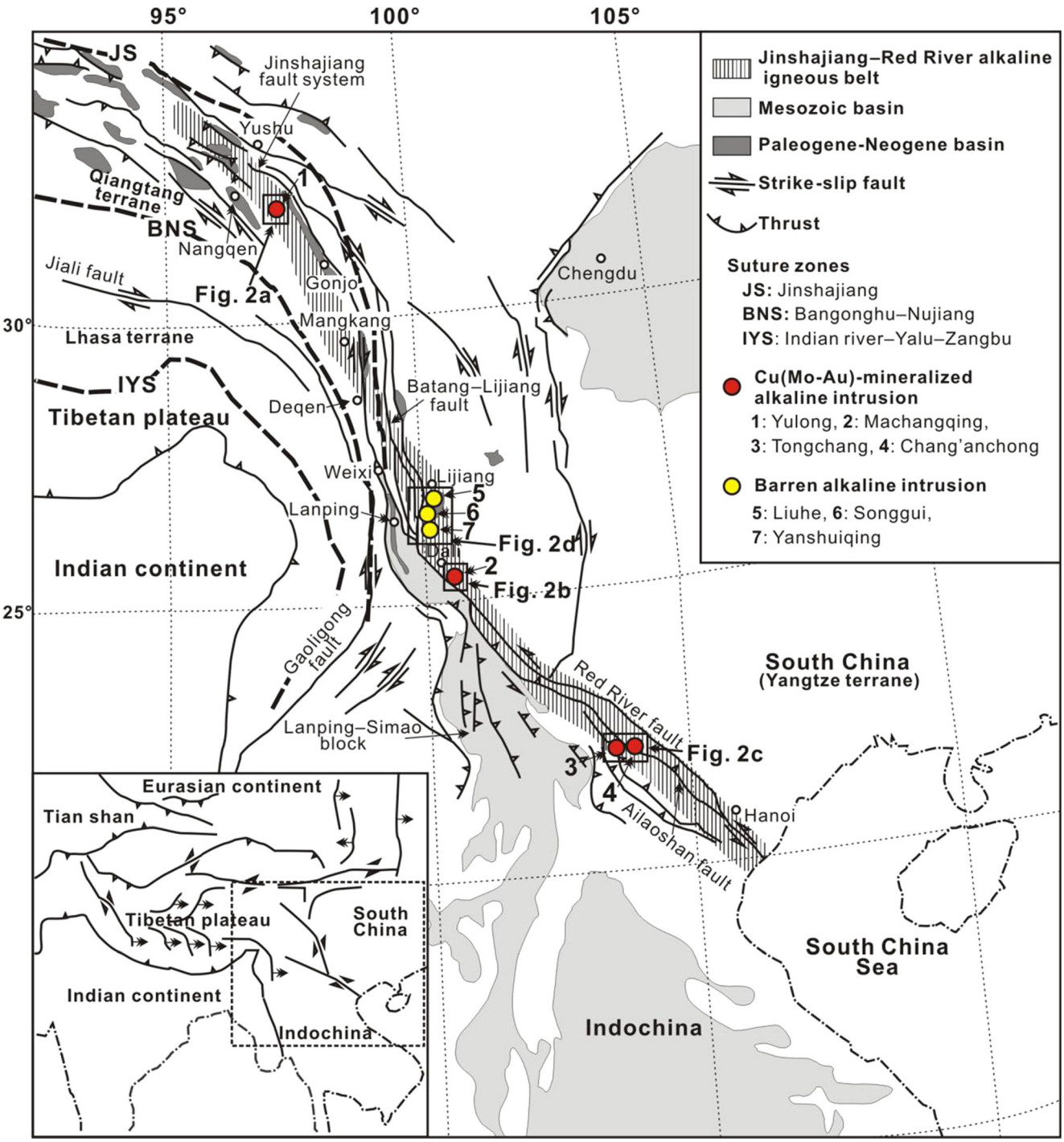

Fig. 1 A simplified geological map of the Jinshajiang–Red River alkaline igneous belt showing Cu-mineralized and barren alkaline intrusions (modified from Wang et al. 2001)

porphyry has phenocrysts of K-feldspar, plagioclase, quartz, hornblende and biotite in a phanerocrystalline groundmass (Fig. 3a). Titanite, zircon and apatite are the main accessory minerals.

The Machangqing deposit is situated in the central area of the Jinshajiang–Red River alkaline igneous belt (Fig. 1). Cu (Mo-Au)-mineralization at the Machangqing deposit was related to the ~35 Ma granite porphyry stock with an outcrop area of 1.3 km^2 (Fig. 2b; Liang et al. 2006b; Xu et al. 2012a), which intruded into lower Ordovician and lower Devonian limestone and sandstone (Xu et al. 2012a). The Machangqing granite porphyry has phenocrysts of K-feldspar, plagioclase, quartz, hornblende and biotite in a phanerocrystalline groundmass (Fig. 3b). Titanite, zircon and apatite are the main

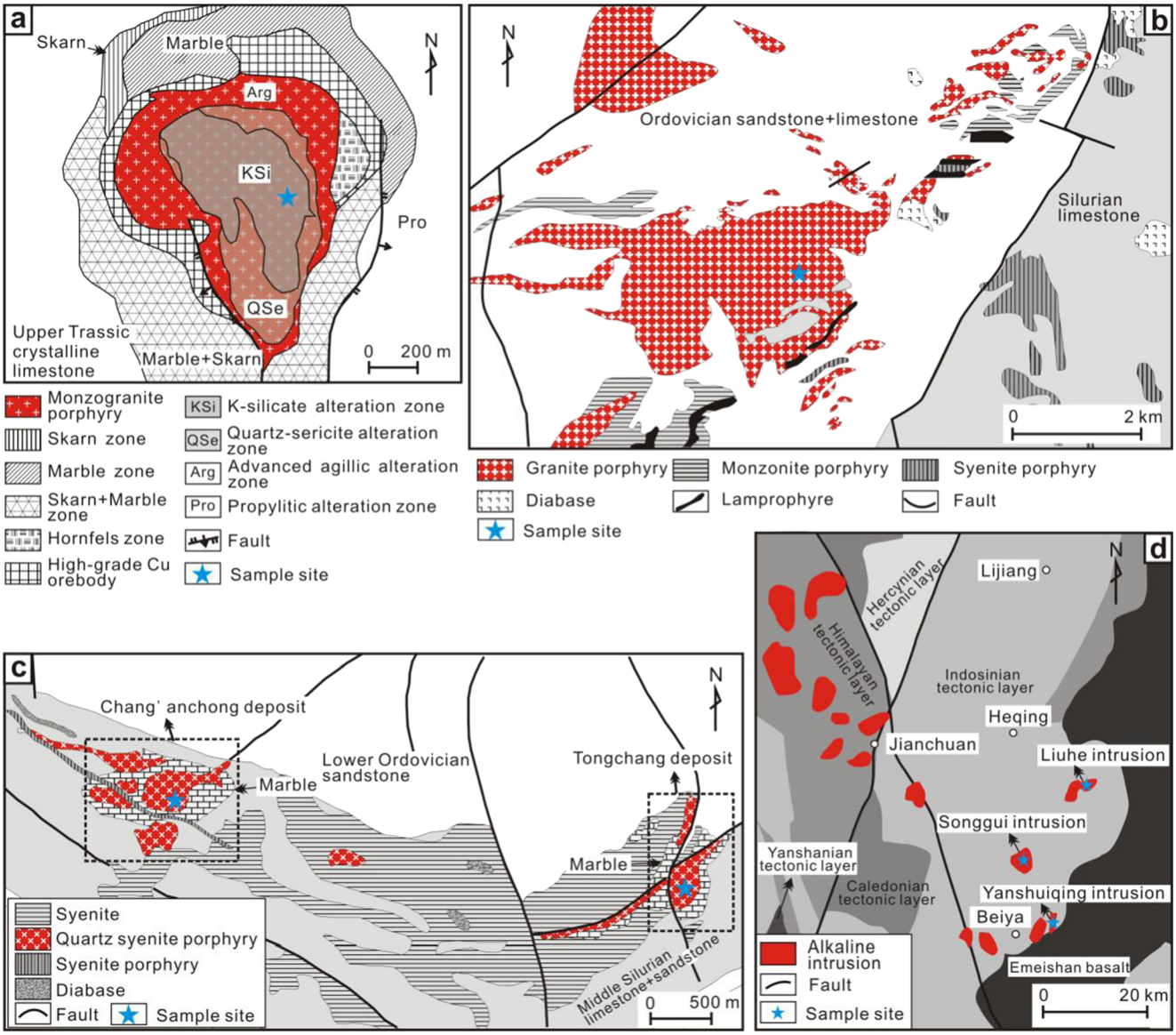

Fig. 2 Simplified geological maps of (**a**) the Yulong deposit (modified from Hou et al. 2006), (**b**) Machangqing deposit (modified from Li 2009), (**c**) Tongchang and Chang'anchong deposits (modified from Xue 2008), and (**d**) Liuhe, Songgui and Yanshuiqing alkaline intrusions (modified from Zhao et al. 2003)

accessory minerals. The deposit contains ~0.25 Mt Cu with 0.44 wt.% Cu, 0.03 wt.% Mo and 0.03 g/t Au (Hou et al. 2006; Xu et al. 2012a).

The Tongchang and Chang'anchong deposits are situated in the southern segment of the Jinshajiang–Red River alkaline igneous belt (Fig. 1). Tongchang is located about 5 km east of Chang'anchong. Cu (Mo-Au)-mineralization at both deposits is associated primarily with ~35 Ma quartz syenite porphyry intrusions (Fig. 2c; Huang et al. 2009; Xu et al. 2012a), which were emplaced into middle Silurian limestone and sandstone. The intrusions form stocks and dykes with outcrop areas of ~0.2 km^2 and >0.18 $km^2$for the Tongchang and Chang'anchong deposits, respectively (Xu et al. 2012a). Both the Tongchang and Chang'anchong quartz syenite porphyries have phenocrysts of K-feldspar, plagioclase, quartz, hornblende and biotite in a phanerocrystalline groundmass (Fig. 3c and d). Titanite, zircon and apatite are the main accessory minerals. The quartz syenite porphyries forming the two deposits may have originated from a shared magma source, as suggested by the similar mineral assemblages, major- and trace-element, and Sr–Nd isotopic compositions, and zircon U–Pb ages (Xu 2011). Tongchang contains 8,621 t Cu and 17,060 t Mo with 1.24 wt.% Cu, 0.218 wt.% Mo and 0.13 g/t Au, whereas Chang'anchong contains 29,337 t Cu and 13,310 t Mo with 1.48 wt.% Cu, 0.13 wt.% Mo and 0.25 g/t Au (Xue 2008).

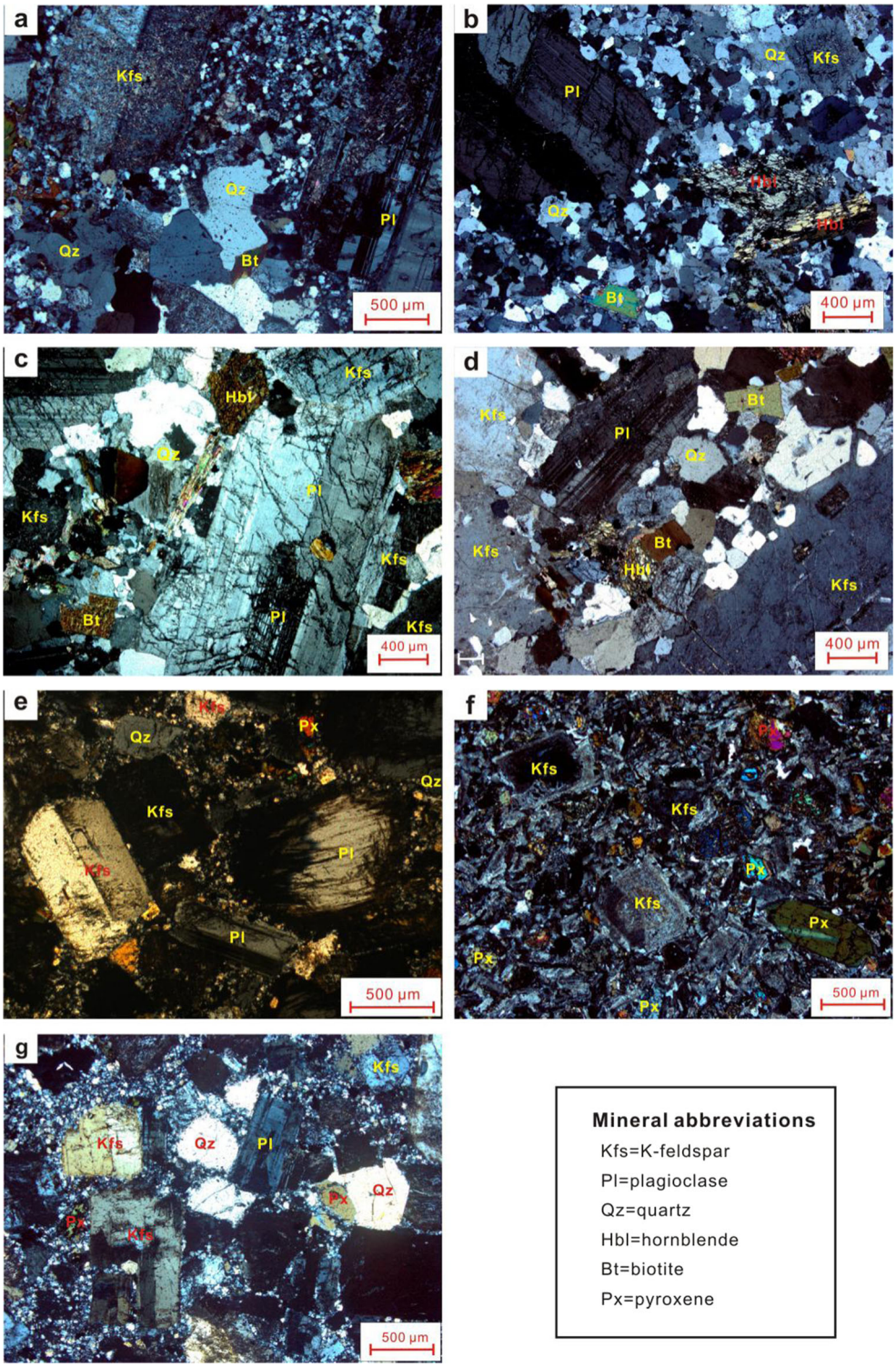

Fig. 3 Photomicrographs showing the textural features and mineral compositions of the Yulong monzongranite porphyries (**a**), Machangqing granite porphyries (**b**), Tongchang quartz syenite porphyries (**c**), Chang'anchong quartz syenite porphyries (**d**), Songgui syenite porphyries (**e**), Liuhe syenite porphyries (**f**) and Yanshuiqing syenite porphyries (**g**)

Liuhe, Songgui and Yanshuiqing barren alkaline intrusions

Between Dali in the south and Lijiang in the north, the Jinshajiang–Red River alkaline igneous belt contains a group of barren alkaline porphyry intrusions of Cenozoic age. The alkaline porphyry intrusions in this group generally occur as stocks and dykes, which intruded into the Caledonian to Himalayan tectonic layers (Fig. 2d). Tectonically, these porphyry intrusions are located in the central part of the Jinshajiang–Red River alkaline igneous belt (Fig. 1). From south to north, this group comprises the Yanshuiqing, Songgui and Liuhe syenite porphyry intrusions (Fig. 2d) , which have

outcrop areas of ~15 km^2, ~25 km^2 and ~25 km^2, respectively (Xu et al. 2014). Both the Yanshuiqing and Songgui syenite porphyries have phenocrysts of major K-feldspar, plagioclase, pyroxene and quartz, and minor hornblende in a phanerocrystalline groundmass (Fig. 3e and f). Zircon U–Pb ages for the Yanshuiqing and Songgui porphyries are ~37 Ma and ~39 Ma, respectively (Xu 2011). The ~37 Ma Liuhe syenite porphyry (Xia et al. 2005; Xu 2011) has phenocrysts of K-feldspar, plagioclase and pyroxene, and minor biotite and hornblende in a phanerocrystalline groundmass (Fig. 3g). Titanite, zircon and apatite are the principal accessory minerals. Various xenoliths have been incorporated into the Liuhe syenite porphyry intrusion, including mainly garnet diopside gneiss and garnet diopside amphibolite, most likely derived from the lower crust (Zhao et al. 2003).

Sampling and analytical methods

Seven titanite-bearing magmatic rock samples, selected from four Cu-mineralized and three barren alkaline porphyry intrusions (Figs. 1 and 2) were investigated in this study. Titanite grains from the samples were prepared as standard petrographic polished thin sections. Optical microscopy and backscattered electron (BSE) imaging were used to determine the shape and internal structure of the titanite grains prior to LA-ICP-MS analysis. BSE imaging was carried out using EPMA (EPMA-1600, Shimadu, Japan) at the State Key Laboratory of Ore Deposit Geochemistry, Institute of Geochemistry, Chinese Academy of Sciences, Guiyang, China.

Major- and trace-element analyses of titanites were obtained directly from polished thin sections using laser-ablation inductively coupled plasma-mass spectrometer (LA-ICP-MS) housed in the State Key Laboratory of Geological Processes and Mineral Resources, China University of Geosciences (Wuhan), China. Detailed operating conditions for the instrumentation and data reduction are described in Liu et al. (2008). Laser sampling was performed using a GeoLas 2005. The diameter of the laser spot was 44 μm. An Agilent 7500a ICP-MS instrument was used to acquire ionsignal intensities. Helium was used as a carrier gas. Argon was used as the make-up gas and mixed with the carrier gas via a T-connector before entering the ICP. Nitrogen was added into the central gas flow (Ar+He) of the Ar plasma to decrease the detection limit and improve precision (Hu et al. 2008). Each analysis incorporated a background acquisition of approximately 20–30 s (gas blank) followed by 50 s data acquisition from the sample. Agilent Chemstation was utilized for the acquisition of each individual analysis. Off-line selection and integration of background and analysis signals, and time-drift correction and quantitative calibration were performed by ICPMSDataCal (Liu et al. 2008). Element contents (major and trace elements) of titanite were obtained using the method similar to that for anhydrous silicate minerals described by Liu et al. (2008). The USGS reference glasses BCR-2G, BHVO-2G and BIR-1G were used as reference materials for external calibration of element contents; ^{29}Si was used as normalizing element and the sum of all metal oxides was normalized to 100 wt.% (Liu et al. 2008). The technique used here was not applied to titanite previously and is thus untested. Therefore, in order to evaluate the reliability of major-element data by LA-ICP-MS, major element coompositions of several titanite grains analysed by LA-ICP-MS from sample YL907 were measured by EMPA (EPMA-1600, Shimadu, Japan) at the State Key Laboratory of Ore Deposit Geochemistry, Institute of Geochemistry, Chinese Academy of Sciences. The results (see Appendix A and Table 1) indicate that among major elements the largest errors are associated with LA-ICP-MS values for Si (9.3 %) and Al (7.5 %) and Ti (3.5 %). These differences would lead to propagated systematic errors of ~5 % for the reported trace element concentrations. Analyses of BCR-2G, BHVO-2G and BIR-1G reference glasses (see Appendix B) as unknown samples are generally consistent with recommended values (http://georem.mpch-mainz.gwdg.de/) within 10 % for most of trace elements. However, due to significant matrix differences between basaltic glasses and titanite, the errors caused by the matrix differences between calibration standards and the unknowns are difficult to estimate. Given that the differences in elemental concentrations in titanite as determined in our study often exceed an order of magnitude, we are confident that our analytical results reflect real variations in sample compositions.

Results

Petrography of titanite

Titanite grains from the mineralized intrusions are mainly yellow/brown in colour varying in size between 200–2000 μm (Fig. 4). They appear homogeneous in transmitted light, and occur mostly as euhedral to subhedral grains, and partially as crystallographic twins, which are adjacent to, or included in, hornblende, biotite, plagioclase, K-feldspar and quartz (Fig. 4). Some titanite grains from the mineralized intrusions are in contact with chlorite formed by alteration of hornblende or biotite, and the BSE images indicate that some titanite grains from the mineralized intrusions contain very small mineral inclusions, but they demonstrate no evidence of inheritance, zoning or overgrowth textures that would indicate multiple periods of mineral growth or resorption (Figs. 4 and 5; Storey et al. 2007; Li et al. 2010). However, titanite grains from the barren intrusions are primarily pale in colour with relatively smaller sizes of 100–200 μm (Fig. 4). They also appear homogeneous in transmitted light and occur mostly as euhedral to subhedral grains or as crystallographic twins,

Table 1 Comparison between EMPA and LA-ICP-MS major element analyses of titanite from sample YL907

No. of analyses	Average EMPA (wt.%) 10	RSD (%)	Average LA-ICP-MS (wt.%) 21	RSD (%)	Difference (%)
TiO_2	38.57	1.64	39.93	1.23	3.51
SiO_2	29.03	0.90	26.34	0.76	9.26
CaO	27.27	1.77	27.16	1.25	0.43
Al_2O_3	1.36	12.80	1.46	9.40	7.47
Na_2O	0.02	181.79	0.02	82.49	22.50
K_2O	0.00	127.41	0.01	208.57	88.02
MnO	0.09	33.19	0.11	4.12	19.85
Fe_2O_3	1.66	14.38	1.68	8.25	1.20
MgO	0.01	134.88	0.02	34.70	47.26
P_2O_5	0.06	30.85	0.06	44.11	4.08
Total	98.07	–	96.78	–	–

which are mainly adjacent to, or included in, plagioclase K-feldspar, pyroxene and quartz (Fig. 4). Whereas some titanite grains from the barren intrusions are in contact with chlorite formed by alteration of pyroxene, and the BSE images indicate that some titanite also contain very small mineral inclusions, we found no evidence of inheritance, zoning or overgrowth textures that would indicate multiple periods of mineral growth or resorption (Fig. 5; Storey et al. 2007; Li et al. 2010).

Chemical compositions of titanite

Mean major- and trace-element compositions of titanite samples are presented in Table 2 and plotted in Figs. 6, 7 and 8. Detailed results of major and trace elements of titanite samples are listed in Appendixes A and B, respectively.

Major-element compositions of titanite

Titanites from the mineralized intrusions have relatively uniform major element compositions (Table 1), whereas titanites from the barren intrusions exhibit larger variations (Fig. 6a, b and d; Table 2). In addition, titanites from both mineralized and barren intrusions have variable Na_2O and MgO contents (Fig. 6c and e; Table 2).

Trace-element compositions of titanite

Titanites from the mineralized intrusions show REE+Y patterns with enrichment in LREEs, depletion in HREEs, notable negative Eu and Y anomalies and weakly positive Ce anomalies on the chondrite-normalized plots (Fig. 7a). They have total REE plus Y contents (ΣREE+Y) ranging from 14,249 to 40,420 ppm (average 28,326 ppm), LREE/HREE ratios from 5.01 to 12.9 (average 8.21), Eu/Eu* values from 0.49 to 0.88 (average 0.67), Ce/Ce* values from 1.14 to 1.38 (average 1.23) and Y/Y* values from 0.71 to 1.02 (average 0.85) (Table 2). They have concentrations of 62.1–248 ppm U (average 122 ppm), 337–985 ppm Th (average 618 ppm), 93.0–500 ppm Ta (average 253 ppm), 989–4097 ppm Nb (average 2082 ppm), 40.5–203 ppm Sr (average 101 ppm) and 29.6–128 ppm Ga (average 77.9 ppm) (Table 2). Th/U ratios are 3.72–7.31 (average 5.18), Nb/Ta ratios are 5.78–11.3 (average 8.52), and Zr/Hf ratios are 10.6–17.5 (average 14.3).

Titanites from the barren intrusions also show REE+Y patterns with enrichment in LREEs, depletion in HREEs, notable negative Eu and Y anomalies and weakly positive Ce anomalies on the chondrite-normalized plots (Fig. 7a), but they have lower ΣREE+Y of 2322–10,954 ppm (average 5586 ppm), lower LREE/HREE ratios of 1.77–7.04 (average 4.49), and higher Eu/Eu* values of 0.73–0.99 (average 0.86), whereas Ce/Ce* values (1.11–1.28; average 1.19) and Y/Y* values (0.62 to 1.00; average 0.79) are similar (Table 2). Concentrations of other trace elements are also lower: 6.48–109 ppm U (average 41.1 ppm), 6.90–270 ppm Th (average 119 ppm), 21.3–139 ppm Ta (average 65.7 ppm), 171–1898 ppm Nb (average 1018 ppm), 66.3–620 ppm Sr (average 255 ppm) and 6.31–32.6 ppm Ga (average 15.3 ppm) (Table 2). Although Th/U ratios are similar between the two intrusion types (3.72–7.31; average 5.18 in the barren intrusions), Nb/Ta ratios and Zr/Hf ratios are different (8.03–29.9; average 15.5 and 10.4–38.4; average 19.7, respectively).

Discussion

Compositional comparisons of titanites between Cu-mineralized and barren intrusions

Major-element compositional results indicate that titanites from the mineralized intrusions have higher Fe_2O_3/Al_2O_3

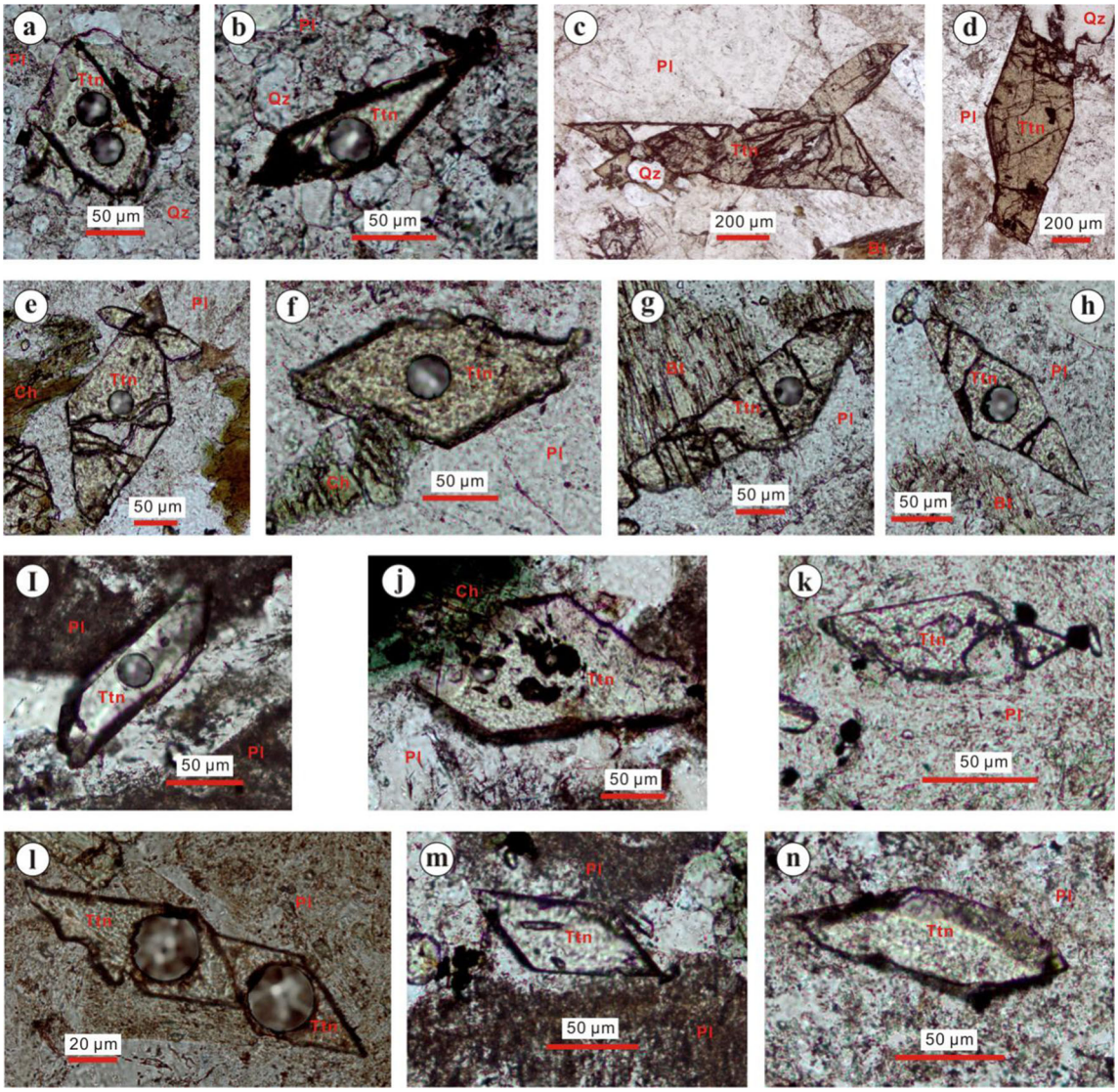

Fig. 4 Photomicrographs showing the occurrences of representative titanite grains from the: Yulong monzongranite porphyries (**a**, **b**), Machangqing granite porphyries (**c**, **d**), Tongchang quartz syenite porphyries (**e**, **f**), Chang'anchong quartz syenite porphyries (**g**, **h**), Songgui syenite porphyries (**i**, **j**), Liuhe syenite porphyries (**k**, **l**), and Yanshuiqing syenite porphyries (**m**, **n**). Mineral abbreviations: *Pl* plagioclase; *Ttn* titanite; *Qz* quartz; *Bt* biotite; *Ch* chlorite

ratios, and lower Al_2O_3 and CaO contents than those from the barren intrusions (Fig. 6a and f). The trace-element compositions of titanites from the mineralized and barren intrusions display large variations (Table 2 and Appendix B), demonstrating that titanite is capable of accommodating a wide range of trace elements (Higgins and Ribbe 1976; Deer et al. 1982; Cérny' et al. 1995; Frost et al. 2000). Furthermore, titanites from mineralized and barren intrusions can be distinguished on basis of trace-element concentrations and ratios, (such as ΣREE+Y, LREE/HREE, Eu/Eu*, U, Th, Ta, Nb, Ga, Sr, Nb/Ta and Zr/Hf, etc.; Figs. 7 and 8).

Titanites from both the mineralized and barren intrusions show REE+Y patterns with enrichment in LREEs and depletion in HREEs, notable negative Eu and Y anomalies and weakly positive Ce anomalies on the chondrite-normalized plots, but titanites from the mineralized intrusions have much higher ΣREE+Y contents, higher LREE/HREE ratios, obviously larger negative Eu anomalies and slightly larger positive Ce anomalies than those for titanites from the barren intrusions (Figs. 7a, b and c). In addition, the Eu/Eu*–Ce/Ce* diagram also highlights a negative correlation between Eu/Eu* and Ce/Ce*(Fig. 7c), and titanites from the mineralized intrusions show higher (Ce/Ce*)/(Eu/Eu*) ratios than those from the barren intrusions (Fig. 7d).

Uranium and Th concentrations in titanites from the mineralized intrusions are notably higher than those for titanites from the barren intrusions, and the two types of titanites can be distinguished from each other on the Th–U diagram (Fig. 8a). Tantalum and Nb in titanites from the mineralized intrusions are extremely enriched, demonstrating that titanite is an

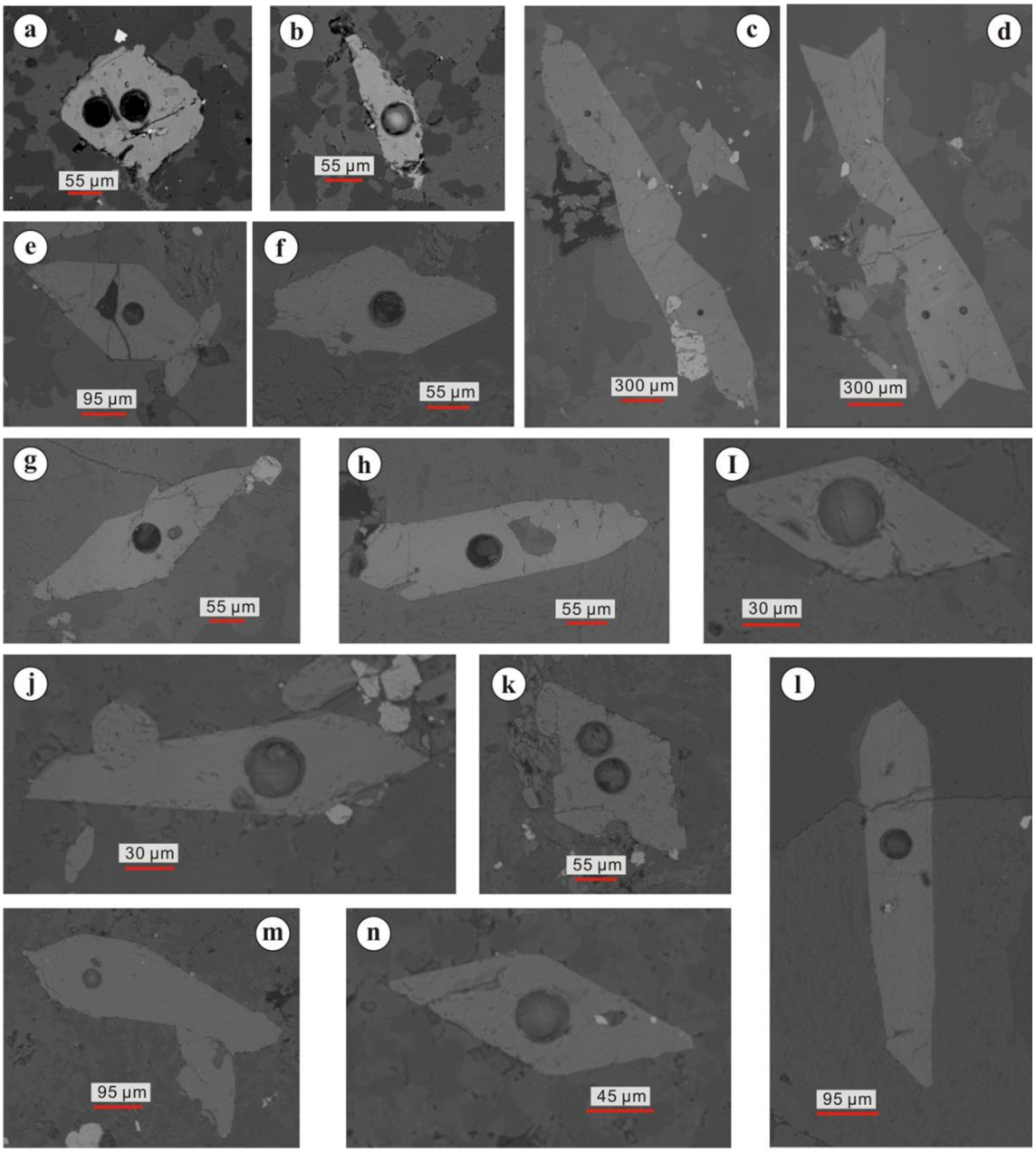

Fig. 5 Backscattered electron images showing morphological and textural features of representative titanite grains from the: Yulong monzongranite porphyries (**a**, **b**), Machangqing granite porphyries (**c**, **d**), Tongchang quartz syenite porphyries (**e**, **f**), Chang'anchong quartz syenite porphyries (**g**, **h**), Songgui syenite porphyries (**i**, **j**), Liuhe syenite porphyries (**k**, **l**), and Yanshuiqing syenite porphyries (**m**, **n**)

important host for Ta and Nb, which are much higher than those for titanites from the barren intrusions. Furthermore, titanites from the mineralized and barren intrusions have different enrichment trends for Nb–Ta and Zr–Hf (Fig. 8b and c), consequently producing both lower Zr/Hf and Nb/Ta ratios for titanites from the mineralized intrusions, which can be easily distinguished from titanites from the barren intrusions (Fig. 8d). In addition, titanites from the mineralized and barren intrusions show different enrichment trends for Sr and Ga (Fig. 8e and f). Strontium in titanites from barren intrusions is much higher than in titanites from the mineralized intrusions (Fig. 8e), whereas Ga in titanites from mineralized intrusions is significantly higher than in titanites from the barren intrusions (Fig. 8f).

Possible factors causing compositional differences of titanites between Cu-mineralized and barren intrusions

TiO_2 contents of titanites from both the mineralized and barren intrusions have negative correlations with Al_2O_3+ Fe_2O_3 (Fig. 9a), indicating the substitution $(Fe, Al)^{3+} + (OH, F)^{-} \Longleftrightarrow Ti^{4+} + O^{2-}$ (Frost et al. 2000, and references therein).

Table 2 Mean major- and trace-element compositions of titanite samples from Cu-mineralized and barren intrusions from the Jinshajing–Red River alkaline igneous belt

Intrusion	Cu-mineralized intrusions												Barren intrusions								
	Yulong			Machangqing			Tongchang			Chang'anchong			Liuhe			Songgui			Yanshuiqing		
Sample	YL907			MCQ920			TC904			CAC906			LH07			SG05			YS05		
	Mean	Max.	Min.	Mean	Max.	Min.	Mean	Max.	Min.	Mean	Max.	Min.	Mean	Max.	Min.	Mean	Max.	Min.	Mean	Max.	Min.
Major element (wt.%)																					
TiO_2	39.93	40.85	39.26	38.87	39.39	37.87	38.24	39.11	37.22	39.28	39.94	38.37	39.11	42.22	35.39	37.67	39.53	35.33	37.78	39.40	36.36
SiO_2	26.34	26.72	25.93	26.77	27.15	26.27	26.03	26.90	25.13	26.36	26.79	26.01	27.43	28.11	26.68	27.73	28.28	26.83	27.71	28.97	26.73
CaO	27.16	27.82	26.58	26.78	27.35	25.88	26.59	27.24	25.99	26.51	27.29	25.83	28.44	29.79	27.90	28.48	29.05	27.46	28.39	28.73	27.47
Al_2O_3	1.46	1.71	1.16	1.44	1.75	1.26	1.64	1.89	1.44	1.53	1.86	1.33	2.26	3.09	1.26	2.71	3.63	1.83	2.69	3.12	2.18
Na_2O	0.02	0.09	0.01	0.02	0.03	0.02	0.05	0.29	0.02	0.03	0.09	0.02	0.05	0.12	0.02	0.04	0.19	0.02	0.04	0.09	0.02
K_2O	0.01	0.05	0.00	0.00	0.00	0.00	0.01	0.04	0.00	0.01	0.09	0.00	0.01	0.04	0.00	0.01	0.14	0.00	0.01	0.03	0.00
MnO	0.11	0.12	0.10	0.14	0.15	0.11	0.13	0.15	0.12	0.12	0.13	0.11	0.08	0.11	0.02	0.09	0.15	0.04	0.10	0.12	0.08
Fe_2O_3	1.68	1.88	1.28	1.82	2.28	1.70	1.98	2.97	1.65	1.76	2.01	1.57	1.33	2.47	0.31	1.90	2.40	0.90	1.88	2.24	1.28
MgO	0.02	0.05	0.01	0.05	0.46	0.02	0.04	0.11	0.02	0.02	0.05	0.02	0.06	0.41	0.01	0.03	0.05	0.02	0.03	0.04	0.01
P_2O_5	0.06	0.17	0.03	0.06	0.08	0.04	0.20	1.12	0.06	0.09	0.17	0.07	0.24	0.95	0.03	0.15	0.42	0.03	0.11	0.36	0.03
Total	96.78	97.77	95.90	95.95	96.65	95.04	94.92	95.59	94.49	95.71	96.32	94.56	99.01	99.46	98.61	98.81	99.19	97.61	98.74	98.99	98.32
Structural formula (apfu) calculated based on Σoxygens= 5																					
Ti	1.023			1.002			0.998			1.015			0.976			0.942			0.946		
Si	0.900			0.920			0.906			0.908			0.913			0.925			0.925		
Ca	0.994			0.986			0.991			0.979			1.014			1.018			1.015		
Al	0.059			0.058			0.067			0.062			0.089			0.106			0.106		
Na	0.002			0.002			0.004			0.002			0.003			0.003			0.002		
K	0.000			0.000			0.000			0.000			0.000			0.000			0.000		
Mn	0.003			0.004			0.004			0.003			0.002			0.003			0.003		
Fe	0.043			0.047			0.052			0.045			0.033			0.048			0.047		
Mg	0.001			0.003			0.002			0.001			0.003			0.002			0.001		
P	0.002			0.002			0.006			0.003			0.007			0.004			0.003		
Σcations	3.025			3.023			3.030			3.020			3.041			3.051			3.049		
Trace element (ppm)																					
Ga	65.4	114	29.6	75.1	128	32.6	105	117	84.7	73.8	112	36.0	14.1	21.4	7.63	14.9	27.5	6.31	16.4	32.6	6.32
Sr	78.6	115	45.1	62.3	84.3	40.5	153	203	111	124	176	102	284	517	66.3	264	620	77.6	225	561	78.9
La	1880	2732	994	2172	3141	1242	3045	3942	1804	2208	3238	1494	322	735	106	375	892	158	410	677	224
Ce	7929	11102	4856	9171	12313	5930	11271	13504	7914	9290	12250	6920	1204	2350	523	1445	3333	707	1653	2627	860

Table 2 (continued)

Intrusion	Cu-mineralized intrusions												Barren intrusions								
	Yulong			Machangqing			Tongchang			Chang'anchong			Liuhe			Songgui			Yanshuiqing		
Sample	YL907			MCQ920			TC904			CAC906			LH07			SG05			YS05		
	Mean	Max.	Min.	Mean	Max.	Min.	Mean	Max.	Min.	Mean	Max.	Min.	Mean	Max.	Min.	Mean	Max.	Min.	Mean	Max.	Min.
Pr	1246	1836	748	1517	2153	1092	1839	2213	1307	1602	2102	1222	199	340	96.4	240	531	133	272	410	142
Nd	5790	7924	3352	7129	9024	5790	8485	10727	6105	7872	10820	6548	986	1522	483	1279	2701	746	1363	2031	774
Sm	1117	1481	670	1539	1823	1168	1889	2464	1439	1744	2394	1320	253	375	127	326	621	207	345	463	201
Eu	240	315	158	238	333	168	338	470	237	331	442	262	67.4	104	36.2	89.1	157	60.4	95.9	132	66.6
Gd	786	1100	524	1068	1344	799	1314	1660	1056	1287	1611	1030	235	333	127	306	586	193	338	479	209
Tb	93.3	131	63.2	141	180	107	168	204	134	176	218	143	36.0	50.0	21.2	40.3	70.3	28.0	46.4	62.8	27.6
Dy	560	782	376	852	1156	635	814	979	656	897	1275	636	198	298	123	257	445	183	270	391	181
Ho	81.4	122	63.6	127	156	98.3	142	164	120	128	151	108	33.0	49.4	20.4	42.4	66.8	31.4	46.0	60.2	28.4
Er	219	302	169	334	401	289	324	362	275	339	405	285	78.0	129	44.4	106	148	75.1	112	142	62.9
Tm	25.8	34.9	20.6	39.4	44.0	35.9	44.1	51.2	39.1	38.4	43.6	34.3	10.9	20.6	5.66	12.9	16.8	7.10	14.4	18.2	7.92
Yb	178	229	135	256	300	211	251	272	225	247	292	204	59.1	107	31.1	72.8	119	27.0	89.5	124	48.2
Lu	20.4	24.0	16.9	27.8	31.7	24.3	24.9	31.8	19.1	26.0	29.0	23.1	6.75	11.4	3.28	8.34	11.3	3.66	9.01	11.7	4.39
Y	2472	3553	2025	3633	4237	3118	3613	4180	3144	3647	4214	3180	820	1422	484	1038	1621	683	1228	1479	632
Zr	554	850	377	524	628	465	632	782	521	653	2246	493	835	3174	179	1039	5146	214	891	2381	255
Hf	41.3	79.3	33.1	39.6	44.0	35.4	44.0	70.6	33.6	41.5	136	33.2	31.7	93.3	10.5	51.2	223	12.6	46.7	122	21.9
Nb	1337	1895	988	2303	2801	1591	2314	3523	1696	2339	4097	1746	712	1722	171	1008	1897	435	1245	1832	469
Ta	137	194	93.0	259	314	205	305	500	230	311	467	208	55.1	139	21.3	62.9	130	32.9	76.3	98.5	38.5
Th	486	571	404	614	718	337	767	985	639	637	960	515	76.1	205	6.90	122	270	46.7	146	225	65.9
U	104	143	62.1	106	136	80.5	151	226	118	134	248	107	27.7	68.9	6.48	49.4	109	12.0	41.9	57.7	12.4
ΣREE+Y	22638	30673	14249	28245	35972	23236	33564	40420	25272	29832	38585	24790	4507	7142	2322	5638	10954	3346	6292	8664	3469
LREE/HREE	9.33	12.86	6.85	7.73	9.81	5.01	8.73	10.4	6.86	7.42	9.01	5.46	4.69	7.04	1.77	4.37	6.90	3.22	4.48	6.36	2.82
Eu/Eu*	0.79	0.88	0.69	0.57	0.65	0.49	0.65	0.73	0.55	0.68	0.73	0.63	0.85	0.94	0.76	0.87	0.93	0.79	0.86	0.99	0.73
Ce/Ce*	1.28	1.38	1.18	1.24	1.33	1.16	1.17	1.26	1.14	1.22	1.28	1.15	1.18	1.26	1.11	1.18	1.22	1.13	1.21	1.28	1.16
Y/Y*	0.89	1.02	0.79	0.85	0.95	0.74	0.82	0.91	0.73	0.83	0.94	0.71	0.77	0.89	0.67	0.76	0.94	0.62	0.85	1.00	0.66
No. of analyses	21			25			16			25			12			18			17		

$Eu/Eu^*=Eu_N/(Sm_N\times Gd_N)^{1/2}$, $Ce/Ce^*=Ce_N/(La_N\times Pr_N)^{1/2}$, $Y/Y^*=Y_N/(Dy_N\times Ho_N)^{1/2}$

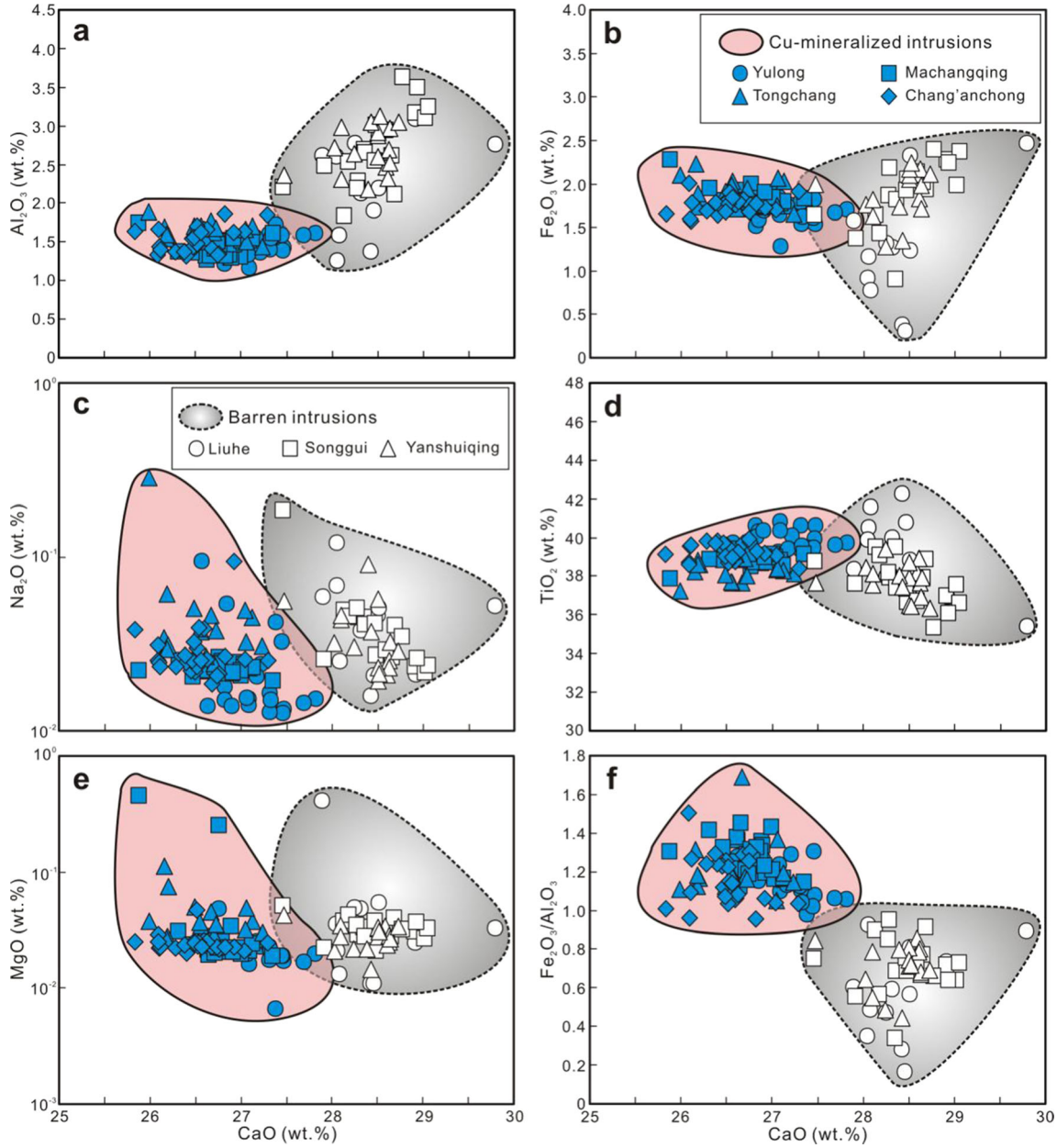

Fig. 6 Plots of CaO vs. Al_2O_3 (**a**), Fe_2O_3 (**b**), Na_2O (**c**), TiO_2 (**d**), MgO (**e**) and Fe_2O_3/Al_2O_3 (**b**) for titanite samples from Cu-mineralized and barren intrusions from the Jinshajiang–Red River alkaline igneous belt (the symbols for intrusions in the following figures are same to those in this figure)

In addition, CaO contents of titanites from both the mineralized and barren intrusions show a negative correlation with Sr^{2+} (Fig. 9e), and the CaO+TiO_2 contents negatively correlate with $\Sigma REY^{3+}+Al^{3+}+Fe^{3+}$, $Na^{+}+Nb^{5+}+Ta^{5+}$ and $U^{4+}+Th^{4+}+Mg^{2+}$ (Fig. 9b, c and d), indicating the likely substitution mechanisms: $Ca^{2+} + Ti^{4+}=REE^{3+} + Y^{3+} + (Al, Fe)^{3+}$, $Ca^{2+} + Ti^{4+}=Na^{+} + (Nb, Ta)^{5+}$, $Ca^{2+}+Ti^{4+}=(U, Th)^{4+} + Mg^{2+}$ and $Ca^{2+}=Sr^{2+}$. Additional possible substitutions include: (1) $(Zr, Hf)^{4+}=Ti^{4+}$; (2) $(Al, Fe)^{3+} + (Nb, Ta)^{5+}=2Ti^{4+}$ (Higgins and Ribbe 1976; Groat et al. 1985; Frost et al. 2000; Tiepolo et al. 2002; Liferovich and Mitchell 2005; Prowatke and Klemme 2005; Aleksandrov and Troneva 2007; Xie et al. 2010; Anand and Balakrishnan 2011; Olin and Wolff 2012).

The darker colour of titanite is suggested to be related to higher Fe/Al ratios (Frost et al. 2000; Aleinikoff et al. 2002). Darker colour titanites from the mineralized intrusions commonly exhibit higher Fe_2O_3/Al_2O_3 ratios than the lighter colour titanite from the barren intrusions, consistent with this suggestion.

Trace-element incorporation in titanite depends upon the crystal-chemical behavior of titanite, coexisting melt compositions and mineral phases, pressure, temperature and fO_2

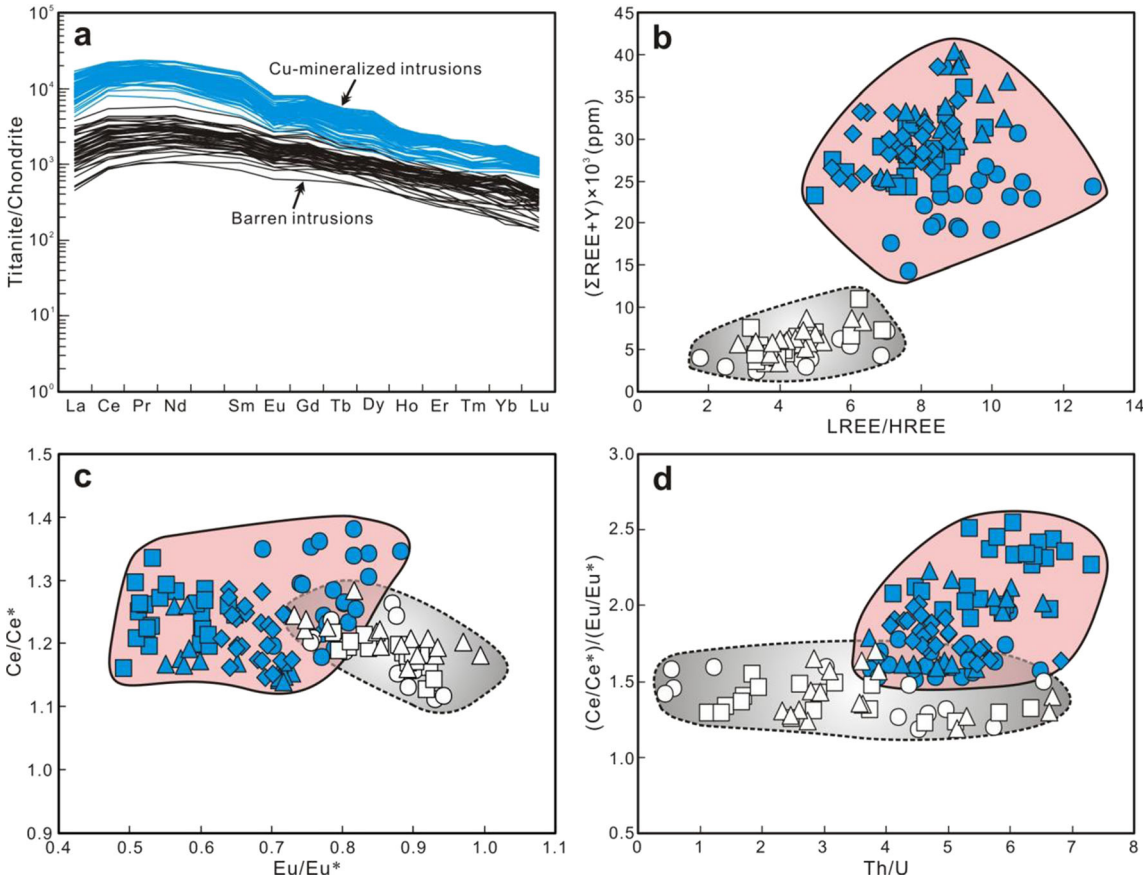

Fig. 7 Chondrite-normalized REY patterns (normalized values for chondrite are from Sun and Mcdoonough 1989) (**a**), and plots of LREE/HREE vs. ΣREE+Y (**b**), Eu/Eu* vs. Ce/Ce* (**c**) and Th/U vs. (Eu/Eu*)/(Ce/Ce*) (**d**) for titanite samples from Cu-mineralized and barren intrusions from the Jinshajiang–Red River alkaline igneous belt

(Watson 1976; Adam and Green 1994; Tiepolo et al. 2002; Prowatke and Klemme 2005, 2006; Jung and Hellebrand 2007; Smith et al. 2009; Anand and Balakrishnan 2011; Olin and Wolff 2012). Concerning the crystal-chemical behavior of titanite, the availability of suitable substitution mechanisms to achieve electrovalent balance and the similarity in size of major- or trace-elements are the main factors (Tiepolo et al. 2002). The coexisting melt compositions and mineral phases, which control the availability of trace-element compositions in melts during titanite growth, thus can exert significant influences on the concentrations and patterns of trace elements in titanite (Watson 1976; Tiepolo et al. 2002; Prowatke and Klemme 2005; Smith et al. 2009; Anand and Balakrishnan 2011; Olin and Wolff 2012). Previous works have indicated that temperature, instead of pressure, has a notably inverse effect on the trace-element concentrations in titanite (Tiepolo et al. 2002; Anand and Balakrishnan 2011). The fO_2 exerts influence mainly on trace elements with different valances such as Ce and Eu (King et al. 2013). In this study, the crystallization temperature of magmas for the mineralized and barren intrusions is likely to be similar, ~750 °C (Xu 2011). As mentioned above, REE+Y, U, Th, Nb, Ta, Zr, Hf and Sr in titanites from the both mineralized and barren intrusions were incorporated through suitable substitution mechanisms. Therefore, these trace-element concentrations in titanites were mainly controlled by availability of trace-element compositions in melts during titanite growth. Plots of ΣREE+Y, LREE/HREE, U, Th, Ta and Nb of titanites vs. those of whole-rock samples produce general positive correlations (Fig. 10a, b, c, d, e and f). We suggest that the coexisting melt compositions, rather than the coexisting mineral phases, exert a more important influence on these trace-element compositions of titanites from both intrusion types.

Our study has identified very high Ga contents in titanites from the mineralized intrusions. Gallium concentrations in whole-rock samples for both the mineralized and barren intrusions are similar and are about 18–20 ppm (Xu 2011; Xu et al. 2014), but Ga concentrations in titanites from the mineralized and barren intrusions are notably different (Fig. 10g), suggesting that Ga concentrations in titanites are not controlled by the coexisting melts. In igneous rocks, Ga is strongly concentrated in Al- and Fe-enriched minerals such as plagioclase, K-feldspar, nepheline, spinel and magnetite (Paktunc and Cabri 1995; Hieronymus et al. 2001; Tu et al. 2003; Luo et al. 2007; Macdonald et al. 2010). The reason is that under oxidizing conditions Ga^{3+} has geochemical

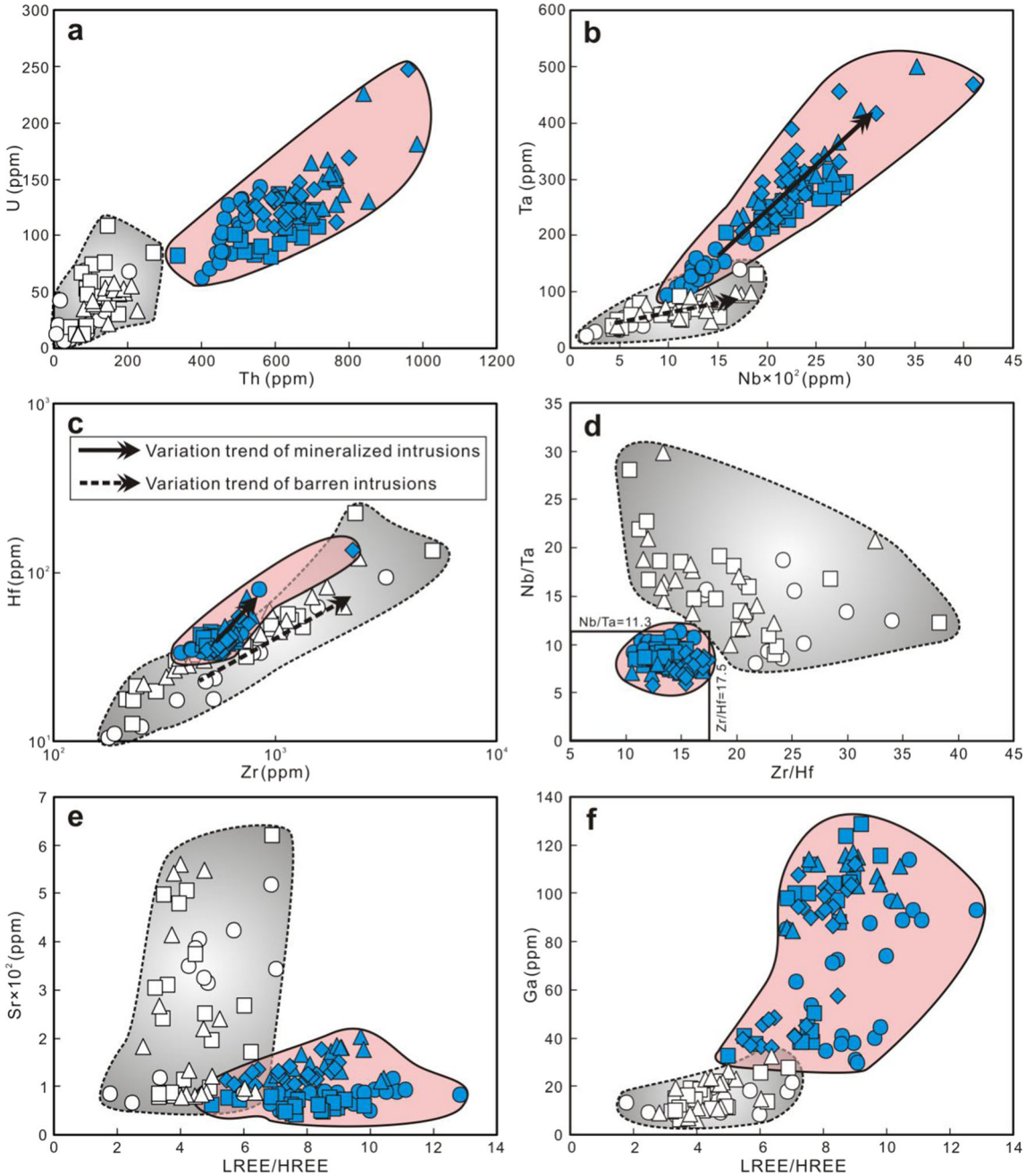

Fig. 8 Plots of Th vs. U (**a**), Nb vs. Ta (**b**), Zr vs. Hf (**c**), Zr/Hf vs. Nb/Ta (**d**), LREE/HREE vs. Sr (**e**), and Ga (**f**) for titanite samples from Cu-mineralized and barren intrusions from the Jinshajiang–Red River alkaline igneous belt

characteristics similar to Al^{3+} and Fe^{3+}, and thus commonly substitutes for Al^{3+} and Fe^{3+} (Tu et al. 2003; Luo et al. 2007; Macdonald et al. 2010; Breiter et al. 2013). As with Al^{3+} and Fe^{3+}, Ga would most likely substitute for Ti in titanite, as deduced from a negative correlation between TiO_2 and Ga (Fig. 9f). Furthermore, effective ionic radius of the hexahedral Ga^{3+} is closer to Ti in titanite than for hexahedral Al^{3+} and Fe^{3+} (Shannon 1976), implying that Ga^{3+} enters titanite more readily than Al^{3+} and Fe^{3+}. Therefore, magmatic fO_2 should be a significant control on Ga uptake by titanite, and the pronounced high Ga concentrations in titanites from the mineralized intrusions suggest oxidized conditions, consistent with conclusion made on the basis of other methods (Liang et al. 2006a, b; Bi et al. 2009; Xu 2011; Xu et al. 2012b, 2014).

In contrast to the barren intrusions, mineralized intrusions have higher Sr concentrations, but contain titanites with lower Sr concentrations (Fig. 10h), indicating that Sr concentrations in titanites do not reflect Sr concentrations in the parental melts. They are probably controlled by the nature of other crystalizing mineral phases. As Sr is compatible in plagiolcse,

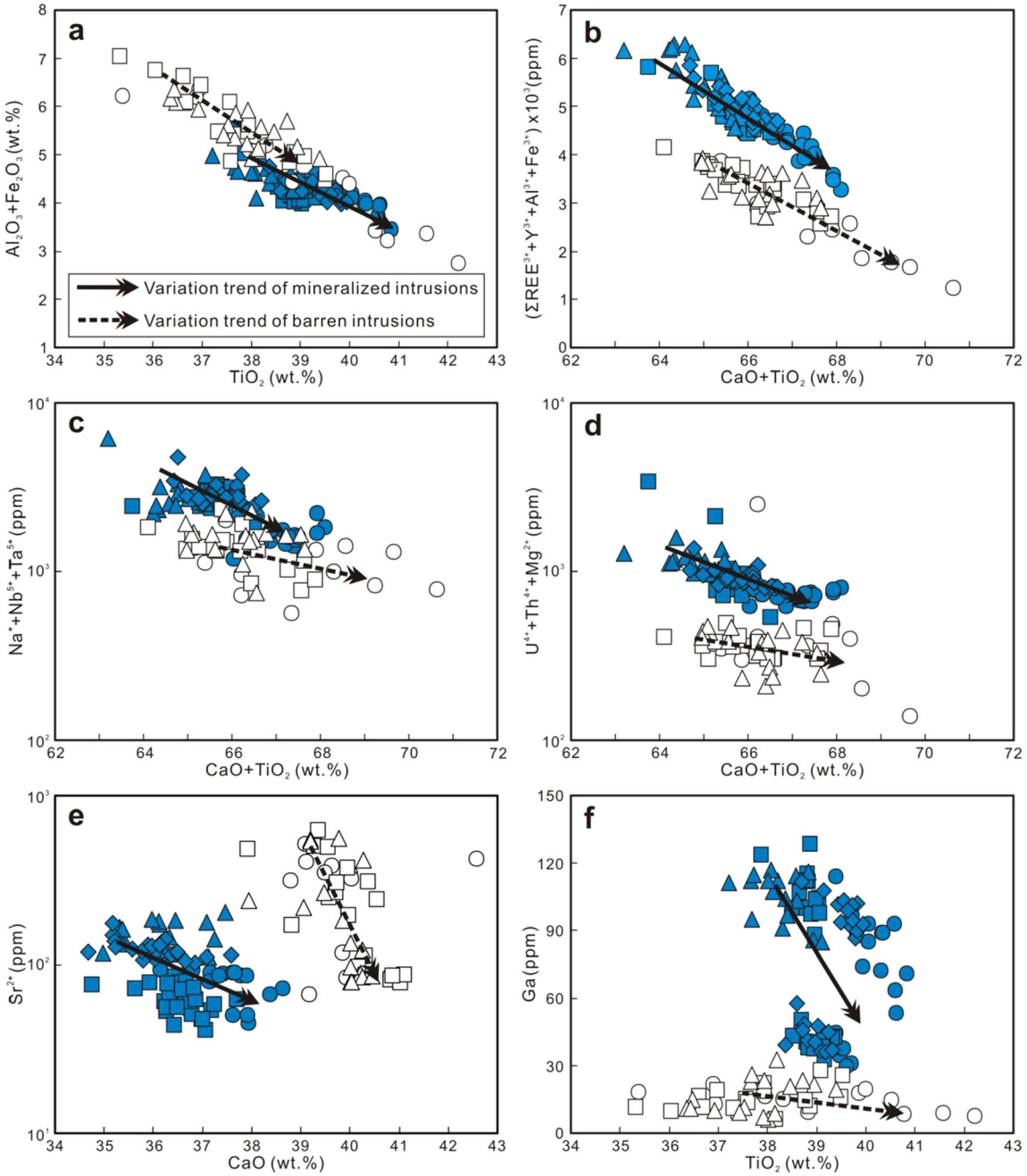

Fig. 9 Plots of TiO_2 vs. $Al_2O_3+Fe_2O_3$ (**a**), and CaO + TiO_2 vs. $\Sigma REE^{3+}+Y^{3+}+Al^{3+}+Fe^{3+}$ (**b**), $Na^{+}+Nb^{5+}+Ta^{5+}$ (**c**) and $U^{4+}+Th^{4+}+Mg^{2+}$ (**d**), and CaO vs. Sr^{2+} (**e**), and TiO_2 vs. Ga (**f**) for titanite samples from Cu-mineralized and barren intrusions from the Jinshajiang–Red River alkaline igneous belt

small proportions of plagioclase crystallization can strongly decrease Sr concentrations in melts (Icenhower and London 1996; White et al. 2003; White 2003; Ren 2004), and consequently, less Sr can be incorporated into titanites. Therefore, lower Sr concentrations in titanites from the mineralized intrusions may be related to a higher proportion of plagioclase crystallization.

Both Eu and Ce have two oxidation states (Eu^{3+}–Eu^{2+} and Ce^{3+}–Ce^{4+}), and variations in fO_2 can change the oxidation state from Eu^{3+} to Eu^{2+} and Ce^{3+} to Ce^{4+}. Like other REEs, trivalant Eu and Ce are most favored in the heptahedral Ca site in titanite (Frost et al. 2000; Tiepolo et al. 2002; King et al. 2013). Under reducing conditions, Eu as Eu^{2+} is not favored by titanite, thus easily producing negative Eu anomalies on the chondrite-nomalized plots (Colombini et al. 2011; Ismail et al. 2013). Therefore larger negative Eu anomalies of titanites from mineralized intrusions should imply more reduced conditions. However, previous studies (Liang et al. 2006a, b; Xu

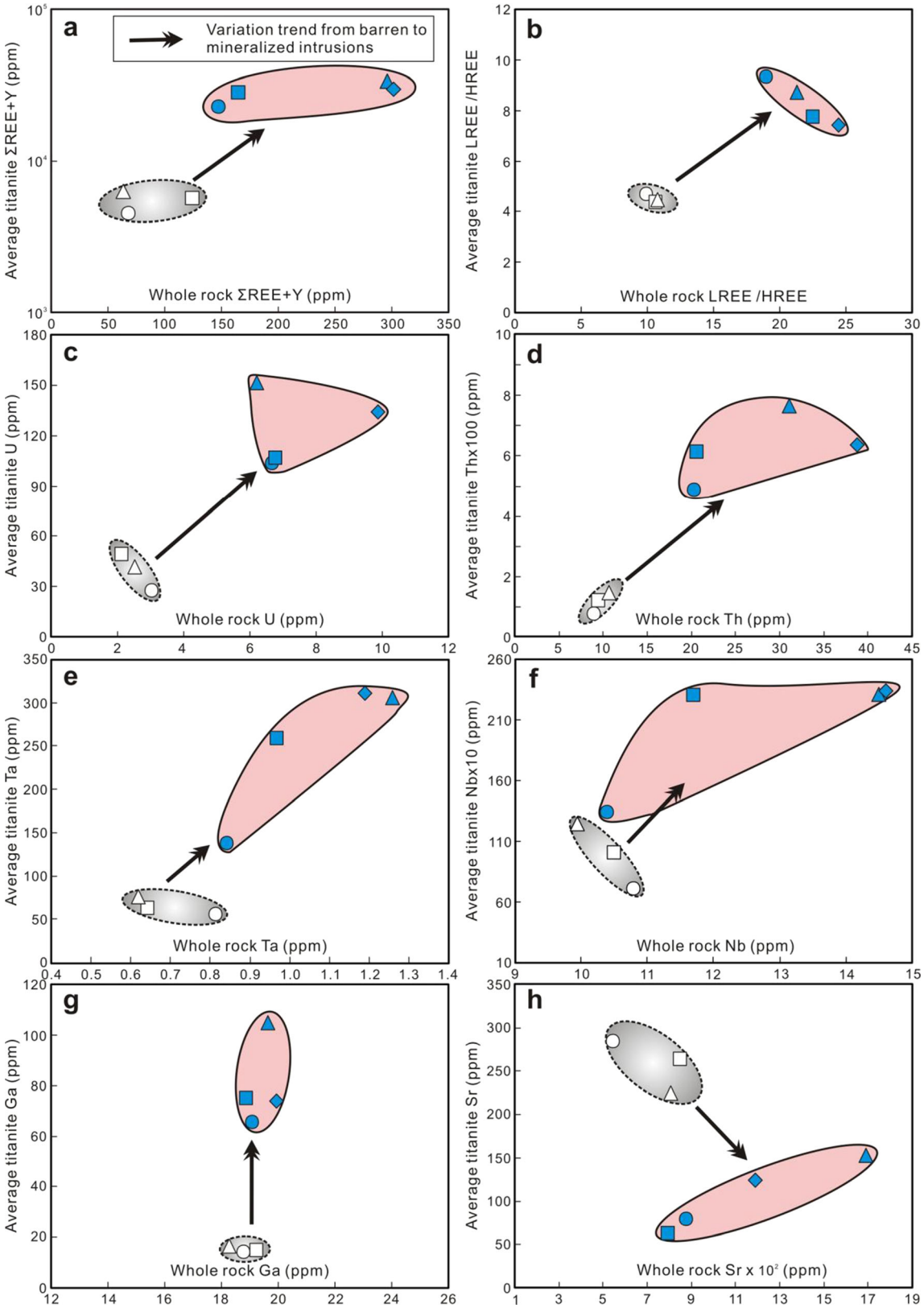

Fig. 10 Plots of ΣREE+Y, LREE/HREE, U, Th, Ta, Nb, Ga and Sr values of titanites vs. those of whole-rock samples (**a**-**h**) for Cu-mineralized and barren intrusions from the Jinshajiang–Red River alkaline igneous belt (trace-element concentrations of whole-rock samples from Xu et al. 2014)

2011; Xu et al. 2012b, 2014) have indicated that mineralized intrusions have higher magmatic fO_2 than barren intrusions. This contradiction can be explained by crystallization of feldspar, because Eu is enriched in plagioclase and minor plagioclase crystallization may produce Eu-depletion in melts (Ballard et al. 2002; Bi et al. 2002; Buick et al. 2010; Anand and Balakrishnan 2011; Ismail et al. 2013). Hence, larger negative Eu anomalies of titanites from the mineralized intrusions may be caused by a larger proportion of plagioclase crystallization, a feature that is consistent with the conclusion made from the lower Sr concentrations in titanites from the mineralized intrusions. Under oxidizing conditions, Ce^{4+} is favored by titanite's hexahedral Ti site (King et al. 2013). Therefore, high fO_2 facilitates incorporation of Ce^{4+} into titanite, readily leading to positive Ce anomalies on the chondrite-nomalized plots. Different degrees of positive Ce anomalies of titanites from the mineralized and barren intrusions are consistent with different magmatic fO_2 conditions for the mineralized and barren intrusions.

Implications for exploration for porphyry Cu deposits

This study has shown that titanites from the Cu-mineralized intrusions have higher values of Fe_2O_3/Al_2O_3, ΣREE+Y, LREE/HREE, Ce/Ce*, (Ce/Ce*)/(Eu/Eu*), U, Th, Ta, Nb and Ga, and lower Al_2O_3, CaO, Eu/Eu*, Sr, Zr/Hf and Nb/Ta values than those for titanites from the barren intrusions. High Ga concentrations and large positive Ce anomalies of titanites from the Cu-mineralized intrusions suggest oxidized conditions, and confirm that an oxidized magma has potential to produce porphyry Cu-mineralization (Ballard et al. 2002; Mungall 2002). Key compositional differences of titanites between the Cu-mineralized and barren intrusions may provide a useful tool to discriminate between ore-bearing and barren intrusions, at an early stage of exploration, and have potential applications in exploration for porphyry Cu deposits in the Jinshajiang – Red River alkaline igneous belt, and other areas.

Conclusions

Titanites from the Cu-mineralized and barren intrusions have different Fe_2O_3/Al_2O_3, Al_2O_3, CaO, ΣREE+Y, LREE/HREE, Ce/Ce*, Eu/Eu*, (Ce/Ce*)/(Eu/Eu*), U, Th, Ta, Nb, Zr/Hf, Nb/Ta, Ga and Sr values. These differences suggest that melts parental to Cu-mineralized and barren intrusions had different chemical compositions and different magmatic fO_2 conditions, and underwent different degrees of crystallization of plagioclase. The Cu-mineralized intrusions are more oxidized. The pronounced compositional differences of titanites between the Cu-mineralized and barren intrusions indicate that titanite has a potential as an indicator for porphyry Cu deposits.

Acknowledgments This research project is financially supported jointly by "the Key Natural Science Foundation of China (41130423), the 12th 5 Year Plan Project of State Key Laboratory of Ore-deposit Geochemistry, Chinese Academy of Sciences (SKLODG-ZY125-03), the Natural Science Foundation of China (41203041, 41473052), the CAS/SAFEA International Partnership Program for Creative Research Teams (Intraplate Mineralization Research Team, KZZD-EW-TZ-20), and the Natural Science Foundation of Guizhou Province ([2012]2335)". Relevant staffs of Yunnan Honghe Henghao Mining Co. Ltd, Yunnan Copper Industry Co. Ltd and Tibet Yulong Copper Industry Co. Ltd. are gratefully acknowledged for their kind help during our fieldwork. Professor Zhaochu Hu (China University of Geociences, Wuhan, China) is thanked for his help in titanite LA-ICP-MS analyses. Professor Ian M Coulson (Regina University, Canada) and Dr. Xiaodong Deng (China University of Geociences, Wuhan, China) are acknowleged for their constructive advice. Associate Editor Leonid Danyushevsky and two anonymous referees are thanked for their constructive review, which significantly improved this paper.

Appendixes

Appendix A

LA-ICP-MS major-element results (wt.%) for titanite samples from Cu-mineralized and barren intrusions from the Jinshajing–Red River alkaline igneous belt

Appendix B

LA-ICP-MS trace-element results (ppm) for titanite samples from Cu-mineralized and barren intrusions from the Jinshajing–Red River alkaline igneous belt

References

Adam J, Green TH (1994) The effect of pressure and temperature on the partitioning of Ti, Sr, and REE between amphibole, clinopyroxene and basanitic melts. Chem Geol 117:219–233

Aleinikoff a JN, Wintsch RP, Fanning M, Dorais MJ (2002) U–Pb geochronology of zircon and polygenetic titanite from the Glastonbury Complex, Connecticut, USA: an integrated SEM, EMPA, TIMS, and SHRIMP study. Chem Geol 188:125–147

Aleksandrov SM, Troneva MA (2007) Composition, mineral assemblages, and genesis of titanite and malayaite in skarns. Geochem Int 45:1012–1024

Anand R, Balakrishnan S (2011) Geochemical and Sm-Nd isotopic study of titanite from granitoid rocks of the eastern Dharwar craton, southern India. J Earth System Sci 120:237–251

Ballard JR, Palin JM, Campbell IH (2002) Relative oxidation states of magmas inferred from Ce(IV)/Ce(III) in zircon: application to porphyry copper deposits of northern Chile. Contrib Mineral Petrol 144:347–364

Belousova EA, Griffin WL, O'Reilly SY, Fisher NI (2002) Apatite as an indicator mineral for mineral exploration: trace-element compositions and their relationship to host rock type. J Geochem Explor 76: 45–69

Bernau R, Franz G (1987) Crystal chemistry and genesis of Nb-, V-, and Al-rich metamorphic titanite from Egypt and Greece. Can Miner 25: 695–705

Bi XW, Hu RZ, Ye ZJ, Shao SX (1999) Study on the relation between the A-type granite and Cu ore mineralization: evidence from the machangqing copper deposit. Sci China (Series D) 29:489–495 (in Chinese)

Bi XW, Cornell DH, Hu RZ (2002) REE composition of primary and altered feldspar from the mineralized alterationn zone of alkali-rich intrusive rocks, western Yunnan Province, China. Ore Geol Rev 19: 69–78

Bi XW, Hu RZ, Cornell DH (2004) Trace element and isotope evidence for the evolution of ore-forming fluid of Yao'an gold deposit, Yunnan Province, China. Miner Depos 39:21–30

Bi XW, Hu RZ, Hanley JJ, Mungall J, Peng JT, Shang LB, Wu KX, Suang Y, Li HL, Hu XY (2009) Crystallisation conditions (T, P, fO_2) from mineral chemistry of Cu- and Au-mineralised alkaline intrusions in the Red River–Jinshajiang alkaline igneous belt, western Yunnan Province, China. Mineral Petrol 96:43–58

Breiter K, Gardenova N, Kanicky V, Vaculovic T (2013) Gallium and germanium geochemistry during magmatic fractionation and post-magmatic alteration in different types of granitoids: a case study from the Bohemian Massif (Czech Republic). Geol Carpath 64:171–180

Buick IS, Hermann J, Maas R, Gibson RL (2007) The timing of sub-solidus hydrothermal alteration in the Central Zone, Limpopo Belt (South Africa): constraints from titanite U-Pb geochronology and REE partitioning. Lithos 98:97–117

Buick IS, Clark C, Rubatto D, Hermann J, Pandit M, Hand M (2010) Constraints on the Proterozoic evolution of the Aravalli-Delhi Orogenic belt (NW India) from monazite geochronology and mineral trace element geochemistry. Lithos 120:511–528

Cao MJ, Li GM, Qin KZ, Seitmuratova EY, Liu YS (2012) Major and trace element characteristics of apatites in granitoids from Central Kazakhstan: implications for petrogenesis and mineralization. Resour Geol 62:63–83

Cérny' P, Novak M, Chapman R (1995) The Al(Nb, Ta)Tiy−2 substitution in titanite: the emergence of a new species? Mineral Petrol 52: 61–73

Che XD, Linnen RL, Wang RC, Groat LA, Brand AA (2013) Distribution of trace and rare earth elements in titanite from tungsten and molybdenum deposits in Yukon and British Columbia, Canada. Can Miner 51:415–438

Chung SL, Lee TY, Lo CH, Wang PL, Chen CY, Yem NT, Hoa TT, Wu GY (1997) Intraplate extension prior to continental extrusion along the Ailao Shan-Red River shear zone. Geology 25:311–314

Chung SL, Lo CH, Lee TY, Zhang YQ, Xie YW, Li XH, Wang KL, Wang PL (1998) Diachronous uplift of the Tibetan plateau starting 40 Myr ago. Nature 394:769–773

Colombini LL, Miller CF, Gualda GAR, Wooden JL, Miller JS (2011) Sphene and zircon in the Highland Range volcanic sequence (Miocene, southern Nevada, USA): elemental partitioning, phase relations, and influence on evolution of silicic magma. Miner Petrol 102:29–50

Deer WA, Howie RA, Zussman J (1982) Rock forming minerals. Orthosilicates, 1A. Longman, London

Ding L, Kapp P, Zhong D, Deng W (2003) Cenozoic volcanism in Tibet: evidence for a transition from oceanic to continental subduction. J Petrology 44:1833–1865

Ding L, Kapp P, Wan XQ (2005) Paleocene-Eocene record of ophiolite obduction and initial India-Asia collision, south central Tibet. Tectonics 24(TC3001):1–18

Frost BR, Chamberlain KR, Schumacher JC (2000) Sphene (titanite): phase relations and role as a geochronometer. Chem Geol 172:131–148

Gao XY, Zheng YF, Chen YX, Guo JL (2012) Geochemical and U-Pb age constraints on the occurrence of polygenetic titanites in UHP metagranite in the Dabie orogen. Lithos 136–139:93–108

Groat LA, Carter RT, Hawthorne FC, Ercitt TS (1985) Tantalian niobian titanite from the Irgon claim, southeastern Manitoba. Can Miner 23: 569–571

Gu XX, Tang JX, Wang CS, Chen JP, He BB (2003) Himalayan magmatism and porphyry copper–molybdenum mineralization in the Yulong ore belt, East Tibet. Mineral Petrol 78:1–20

Hayden LA, Watson EB, Wark DA (2008) A thermobarometer for sphene (titanite). Contrib Mineral Petrol 155:529–540

Hieronymus B, Kotschoubey B, Boulegue J (2001) Gallium behaviour in some contrasting lateritic profiles from Cameroon and Brazil. J Geochem Explor 72:147–163

Higgins JB, Ribbe PH (1976) Crystal-chemistry and space groups of natural and synthetic titanites. Am Miner 61:878–888

Hou ZQ, Ma HW, Zaw K, Zhang YQ, Wang MJ, Wang Z, Pan GT, Tang RL (2003) The Himalayan Yulong porphyry copper belt: product of large-scale strike-slip faulting in eastern Tibet. Econ Geol 98:125–145

Hou ZQ, Zeng PS, Gao YF, Du AD, Fu DM (2006) Himalayan Cu–Mo–Au mineralization in the eastern Indo–Asian collision zone: constraints from Re–Os dating of molybdenite. Miner Depos 41:33–45

Hou ZQ, Pan XF, Yang ZM, Qu XM (2007) Porphyry Cu–(Mo–Au) deposits no related to oceanic-slab subduction: examples from Chinese porphyry deposits in continental setting. Geosci 21:332–351 (in Chinese with English abstract)

Hou ZQ, Zhang HR, Pan XF, Yang ZM (2011) Porphyry Cu(-Mo-Au) deposits related to melting of thickened mafic lower crust: Examples from the eastern Tethyan metallogenic domain. Ore Geol Rev 39: 21–45

Hu RZ, Burnard PG, Turner G, Bi XW (1998) Helium and argon systematics in fluid inclusions of Machangqing copper deposit in west Yunnan province, China. Chem Geol 146:55–63

Hu RZ, Burnard PG, Bi XW, Zhou MF, Pen JT, Su WC, Wu KX (2004) Helium and argon isotope geochemistry of alkaline intrusion-associated gold and copper deposits along the Red River-Jinshajiang fault belt, SW China. Chem Geol 203:305–317

Hu ZC, Gao S, Liu YS, Hu SH, Chen HH, Yuan HL (2008) Signal enhancement in laser ablation ICP-MS by addition of nitrogen in the central channel gas. J Anal Atom Spectro 23:1093–1101

Huang B, Liang HY, Mo JH, Xie YW (2009) Zircon LA-ICP-MS U–Pb age of the Jinping–Tongchang porphyry associated with Cu–Mo mineralization and its geological implication. Geotecton Metallog 33:598–602 (in Chinese with English abstract)

Icenhower J, London D (1996) Experimental partitioning of Rb, Cs, Sr, and Ba between alkali feldspar and peraluminous melt. Am Miner 81:719–734

Ismail R, Ciobanu CL, Cook NJ, Teale GS, Giles D, Mumm AS, Wade B (2013) Rare earths and other trace elements in minerals from skarn assemblages, Hillside iron oxide-copper-gold deposit, Yorke Peninsula, South Australia, Lithos http://dx.doi.org/10.1016/j.lithos.2013.07.023

Jung S, Hellebrand E (2007) Textural, geochronological and chemical constraints from polygenetic titanite and monogenetic apatite from a mid-crustal shear zone: An integrated EPMA, SIMS, and TIMS study. Chem Geol 241:88–107

King PL, Sham TK, Gordon RA, Dyar MD (2013) Microbeam X-ray analysis of Ce^{3+}/Ce^{4+} in Ti-rich minerals: a case study with titanite (sphene) with implications for multivalent trace element substitution in minerals. Am Miner 98:110–119

Li HG (2009) Space-Time framework of structure-magma-minerlaization of alkali-rich porphyry Mo-Cu-Au polymetallic deposit in

Boxingchang, Yunan Province. Ph.D. thesis, China University of Geosciences, Beijing, pp76 (in Chinese with English abstract)

Li JW, Deng XD, Zhou MF, Liu YS, Zhao XF, Guo JL (2010) Laser ablation ICP-MS titanite U-Th-Pb dating of hydrothermal ore deposits: a case study of the Tonglushan Cu-Fe-Au skarn deposit, SE Hubei Province, China. Chem Geol 270:56–67

Li JX, Qin KZ, Li GM, Cao MJ, Xiao B, Chen L, Zhao JX, Evans NJ, McInnes BIA (2012) Petrogenesis and thermal history of the Yulong porphyry copper deposit, Eastern Tibet: insights fromU-Pb and U-Th/He dating, and zircon Hf isotope and trace element analysis. Mineral Petrol 105:201–221

Liang HY, Campbell IH, Allen C, Sun WD, Liu CQ, Yu HX, Xie YW, Zhang YQ (2006a) Zircon Ce^{4+}/Ce^{3+} ratios and ages for Yulong ore-bearing porphyries in eastern Tibet. Miner Depos 41:152–159

Liang HY, Yu HX, Mo CH, Zhang YQ, Xie YW (2006b) Zircon LA-ICP-MS U-Pb age, Ce^{4+}/Ce^{3+} ratios and the geochemical features of the Machangqing complex associated with copper deposit. Chinese J Geochem 25:223–229

Liferovich RP, Mitchell RH (2005) Composition and paragenesis of Na-, Nb- and Zr-bearing titanite from Khibina, Russia, and crysral-structure data for synthetic analogues. Can Miner 43:795–812

Liu YS, Hu ZC, Gao S, Günther D, Xu J, Gao CG, Chen HH (2008) In situ analysis of major and trace elements of anhydrous minerals by LA-ICP-MS without applying an internal standard. Chem Geol 257:34–43

Lucassen F, Franz G, Dulski P, Romer RL, Rhede D (2011) Element and Sr isotope signatures of titanite as indicator of variable fluid composition in hydrated eclogite. Lithos 121:12–24

Luo TY, Dai XD, Zhu D, Tao Y, Song XY, Zhang H (2007) Mineralization of gallium: Implications to Emeishan large igneous province. Acta Mineral Sin 27:281–286 (in Chinese with English abstract)

Macdonald R, Rogers NW, Bagiński B, Dzierżanowski P (2010) Distribution of gallium between phenocrysts and melt in peralkaline salic volcanic rocks, Kenya Rift Valley. Mineral Mag 74:351–363

Marks MAW, Coulson IM, Schilling J, Jacob DE, Schmitt AK, Markl G (2008) The effect of titanite and other HFSE-rich mineral (Ti-bearing andradite, zircon, eudialyte) fractionation on the geochemical evolution of silicate melts. Chem Geol 257:153–172

Massimo C, Urs S, Richard S, Jörn-Freederik W, Maria O (2013) How accurately can we date the duration of magmatic-hydrothermal events in porphyry systems?—an invited paper. Econ Geol 108:566–584

Mo XX, Zhao ZD, Deng JF, Dong GC, Zhou S, Guo TY, Zhang SQ, Wang LL (2003) Response of volcanism to the India-Asia collision. Earth Sci Frontiers 10:135–148 (in Chinese)

Mo XX, Niu YL, Dong GC, Zhao ZD, Hou ZQ, Su Z, Ke S (2008) Contribution of syncollisional felsic magmatism to continental crust growth: a case study of the Paleogene Linzizong volcanic succession in southern Tibet. Chem Geol 250:49–67

Mungall JE (2002) Roasting the mantle: Slab melting and the genesis of major Au and Au-rich Cu deposits. Geology 30:915–918

Olin PH, Wolff JA (2012) Partitioning of rare earth and high field strength elements between titanite and phonolitic liquid. Lithos 128:46–54

Paktunc AD, Cabri LJ (1995) A proton- and electron-microprobe study of gallium, nickel and zinc distribution in chromian spinel. Lithos 35: 261–282

Prowatke S, Klemme S (2005) Effect of melt composition on the partitioning of trace elements between titanite and silicate melt. Geochim Cosmochim Acta 69:695–709

Prowatke S, Klemme S (2006) Rare earth element partitioning between titanite and silicate melts: Henry's law revisited. Geochim Cosmochim Acta 70:4997–5012

Ren MH (2004) Partitioning of Sr, Ba, Rb, Y, and LREE between alkali feldspar and peraluminous silicic magma. Am Miner 89:1290–1303

Scott KM (2005) Rutile geochemistry as a guide to porphyry Cu-Au mineralization, Northparkes, New South Wales, Australia. Geochem-Explor Environ Anal 5:247–253

Shannon RD (1976) Revised effective ionic radii and systematic studies of interatomie distances in halides and chaleogenides. Acta Cryst A32:751–767

Smith MP, Storey CD, Jeffries TE, Ryan C (2009) In situ U-Pb and trace element analysis of accessory minerals in the Kiruna district, Norrbotten, Sweden: New constraints on the timing and origin of mineralization. J Petrol 50:2063–2094

Storey CD, Smith MP, Jeffries TE (2007) In situ LA-ICP-MS U-Pb dating of metavolcanics of Norrbotten, Sweden: Records of extended geological histories in complex titanite grains. Chem Geol 240:163–181

Sun SS, Mcdoonough WF (1989) Chemical and isotopic systematics of oceanic basalts: implication for mantle composition and processes. Geol Soc Specl Publ 42:313–345

Tiepolo M, Oberti R, Vannucci R (2002) Trace-element incorporation in titanite: constraints from experimentally determined solid/liquid partition coefficients. Chem Geol 191:105–119

Tu GZ, Gao ZM, Hu RZ, Zhang Q, Li CY, Zhao ZH et al (2003) Dispersed element geochemistry. Geological Publishing House, Beijing (in Chinese)

Vuorinen JH, Hålenius U (2005) Nb-, Zr- and LREE-rich titanite from the Alnf alkaline complex: Crystal chemistry and its importance as a petrogenetic indicator. Lithos 83:128–142

Wang JH, Yin A, Harrison TM, Grove M, Zhang YQ, Xie GH (2001) A tectonic model for Cenozoic igneous activities in the eastern Indo-Asian collision zone. Earth Planet Sci Lett 88:123–133

Wang DH, Qu WJ, Li ZW, Ying HL, Chen YC (2004) The metallogenic concentrating epoch of the Porphyry Copper (molybdenum) deposits in Jinshajiang–Red River metallogenic belt: Re–Os isotope dating. Sci China (Series D) 34:345–349 (in Chinese)

Wang RC, Xie L, Chen J, Yu AP, Wang LB, Lu JJ, Zhu JC (2012) Tin-carrier minerals in metaluminous granites of the western Nanling Range (southern China): Constraints on processes of tin mineralization in oxidized granites. J Asian Earth Sci. doi:10.1016/j.jseaes.2012.11.029

Watson EB (1976) Two-liquid partition coefficients: experimental data and geochemical implications. Contrib Mineral Petrol 56:119–134

White JC (2003) Trace-element partitioning between alkali feldspar and peralkalic quartz trachyte to rhyolite magma. Part II: Empirical equations for calculating trace-element partition coefficients of large-ion lithophile, high field-strength, and rare-earth elements. Am Miner 88:330–337

White JC, Holt GS, Oarker DF, Ren MH (2003) Trace-element partitioning between alkali feldspar and peralkalic quartz trachyte to rhyolite magma. Part I: Systematics of trace-element partitioning. Am Miner 88:316–329

Xia B, Lin QC, Zhang YQ (2005) Zircon SHRIMP dating of diopsde granite in Ailaoshan-Jinshajiang rock belt and its geological implications—Example for Yuzhaokuai, Matouwan and Shlicun diopsde granites. Geotecton Metallog 29:35–43 (in Chinese with English abstract)

Xie L, Wang RC, Chen J, Zhu JC (2010) Mineralogical evidence for magmatic and hydrothermal processes in the Qitianling oxidized tin-bearing granite (Hunan, South China): EMP and (MC)-LA-ICPMS investigations of three types of titanite. Chem Geol 276:53–68

Xu LL (2011) The diagenetic and metallogenic geochronology and magmatic fO_2 characteristics of Jinshajiang-Red River porphyry Cu (Mo-Au) metallogenic systems. Ph.D. thesis, Institute of Geochemistry, Chinese Academy of Sciences, Guiyang (in Chinese with English abstract)

Xu LL, Bi XW, Hu RZ, Zhang XC, Su WC, Qu WJ, Hu ZC, Tang YY (2012a) Relationships between porphyry Cu–Mo mineralization in the Jinshajiang–Red River metallogenic belt and tectonic activity: constraints from zircon U–Pb and molybdenite Re–Os geochronology. Ore Geol Rev 48:460–473

Xu LL, Bi XW, Chen YW, Qi YQ (2012b) Zircon Ce^{4+}/Ce^{3+} ratios of the Tongchang intrusions in Jinping County, Yunnan Province:

implications for mineralization. Acta Mineral Sin 32:74–82 (in Chinese with English abstract)

Xu LL, Bi XW, Hu RZ, Qi YQ, Tang YY, Wang XS, Zhu JJ (2014) Redox states and genetic mechanism of magmas associated with intra-continental porphyry Cu-Au mineralization within the Jinshajiang–Red River alkaline igneous belt, SW China (under review)

Xue BG (2008) On the division of Au metallogenetic zone and metallogenetic rule in Yunnan. Yunan Geol 27:261–277 (in Chinese with English abstract)

Yin A, Harrison TM (2000) Geologic evolution of the Himalayan–Tibetan orogen. Ann Rev Earth Planet Sci 28:211–280

Zhang YQ, Xie YW (1997) Nd, Sr isotopic character and chronology of Ailaoshan-Jinshajiang alkali-rich intrusive rocks. Sci China (Series D) 27:289–293 (in Chinese)

Zhao X, Mo XX, Yu XH, Lu BX, Zhang J (2003) Mineralogical characteristics and petrogenesis of deep-derived xenoliths in Cenozoic syenite porphyry in Liuhe, western Yunnan Province. Earth Sci Frontiers 10:93–104 (in Chinese with English abstract)